[Frontiers in Bioscience 14, 3419-3454, January 1, 2009]

Roles of translational motion of water molecules in sustaining life

Masahiro Kinoshita

Institute of Advanced Energy, Kyoto University

TABLES OF CONTENTS

1. ABSTRACT

By reviewing the results of our analyses based on statistical-mechanical theories, we point out that the entropic effect arising from the translational motion of water molecules is a principal driving force in a variety of self-assembling and ordering processes in biological systems such as protein folding, molecular recognition, and ordered aggregation of protein molecules. The great entropic loss for the biomolecules accompanying these processes is largely compensated by a great entropic gain of the water that is present in the system. The microscopic mechanisms of protein folding and denaturation, receptor-ligand binding, and amyloid-fibril formation are discussed in detail. We describe an effort to develop a unique method

for predicting the native structure of a protein. The roles of NaCl and cosolute molecules are also briefly discussed.

2. INTRODUCTION

A variety of self-assembling and ordering processes in biological systems, which occur at molecular levels, are sustaining life. Examples of such processes are protein folding leading to a unique native (tertiary) structure, protein traffic, molecular recognition, aggregation of protein molecules forming ordered and often symmetrical (quarterly) structure, and lipid-membrane formation. The key words representing these processes can be "self-assembling", "ordering", "high selectivity", "regularity", and "symmetry". These key words clearly contradict the principle of entropy increase, and the processes appear to occur at the great expense of the system entropy.

Material tends to become highly functional only when it is in contact with or mixed with other material. The behavior of a complex system comprising multiple material constituents is nonlinear in the sense that it is far from the superposition of the behavior of each constituent. In a research of the complex systems, considering each constituent individually is useless, and it is imperative to treat all of the constituents collectively as a system. A biological system is a typical example of the complex systems. Biopolymers, a great diversity of molecular and ionic species, or water is simply *material* when each of them is separately present. However, the complicated correlations among these material constituents can lead to *life*.

Above all, water plays critical roles. A larva of the sleeping chironomid living in Africa synthesizes trehalose when water is lost. Through the glassification of trehalose the larva stops the metabolism and freezes its biological system, waiting for water supply. There is a record that even after seventeen years when the larva was immersed in water it returned to life and began to grow. This is a striking example showing that *life* can be converted to *material* and vice versa and that water is indispensable to life.

It is widely recognized that water plays crucially important roles in the variety of self-assembling and ordering processes mentioned above. In the conventional view, however, the emphasis is placed only on the interaction potentials among the atoms constituting the biomolecules-aqueous solution system. For example, the attractive interaction between a polar or charged group and water is significantly strong or even stronger than the water-water attractive interaction with the result that the group is hydrophilic and preferentially exposed to water. Moreover, most of the water effects are discussed in terms of the interaction potentials. The hydrophobicity of a nonpolar group is considered to be attributable to the asymmetry that the attractive interaction between the group and water is much weaker than the water-water attractive interaction. To oppose the disturbance in the water-water attractive interaction caused by the group, the ordering of water molecules occurs in the vicinity of the group, which leads to an entropic loss. As a consequence, the exposure of the group to water is highly unfavorable. The decrease in the quantity of such entropically unstable water through the burial of nonpolar groups is an essential factor in the biological self-assembly. Though these effects are important, there should be another factor which is missing in the conventional view.

By employing the law of equipartition of energy, we can estimate the root mean square velocity of a water molecule at 298 K: Surprisingly enough, the estimated value reaches ~640 m/sec. How *energetic* the motion of water molecules is! Moreover, those water molecules form dense liquid: The biomolecules are immersed in such hard environments. Of course, the translational motion of a water molecule is remarkably constrained by the other water molecules and the hydrogen bonds. However, the self-diffusion coefficient of water at 298 K and 1 atm is 2.4×10^{-5} cm^2/sec, and the root mean square displacement of water molecules per second is ~0.07 mm that is *macroscopic*.

In this article, we point out that in contrast to the conventional view described above, the entropic effect arising from the translational motion of exceptionally small water molecules which exist as a dense liquid is critical in the self-assembling and ordering processes. These processes certainly accompany a great entropic loss when the attention is paid only to the biomolecules. Based on the results of our detailed analyses using statistical-mechanical theories, we introduce an interesting concept: Most of the entropic loss is compensated by an entropic gain or a free-energy gain originating from the translational motion of the water molecules which are present in the system (not limited to the water molecules near the biomolecules), and the processes are driven primarily by this water-entropy effect. The water entropy emphasized here is the translational entropy (or equivalently, the configurational entropy: a measure of the number of accessible configurations of the water).

3. ENTROPIC EXCLUDED-VOLUME EFFECT

3.1. Asakura-Oosawa theory

As shown in Figure 1(a), the presence of a large particle in small particles generates a space from which centers of the small particles are excluded (the space occupied by the large particle itself plus the space shown in gray). We assume that the small particles are spheres with diameter d_S and the large particles are spheres with diameter d_L: The excluded space is a sphere with diameter "d_S+d_L". If a pair of large spheres contact each other, the two excluded spaces overlap (the overlapped space is shadowed in Figure 1(a)), and the total volume available to the translational motion of small spheres increases by the volume of the overlapped space. This leads to an entropic gain and a free-energy gain of the small spheres. Therefore, an interaction is induced between the large spheres, which drives them to contact each other. Since the interaction is induced even when all of the spheres are hard spheres with no soft potentials (all the allowed system configurations share the same energy and the system behavior becomes

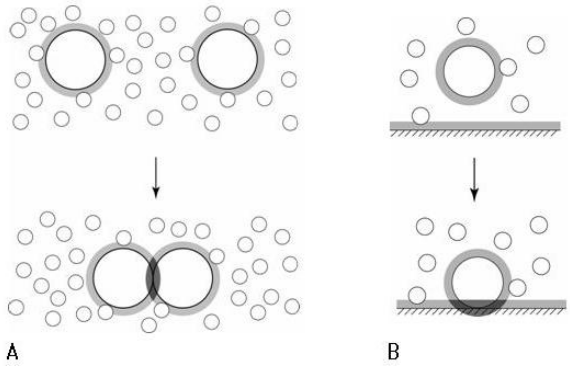

Figure 1. (a) Contact of large spheres immersed in small spheres. (b) Contact of a large sphere and a planar wall immersed in small spheres.

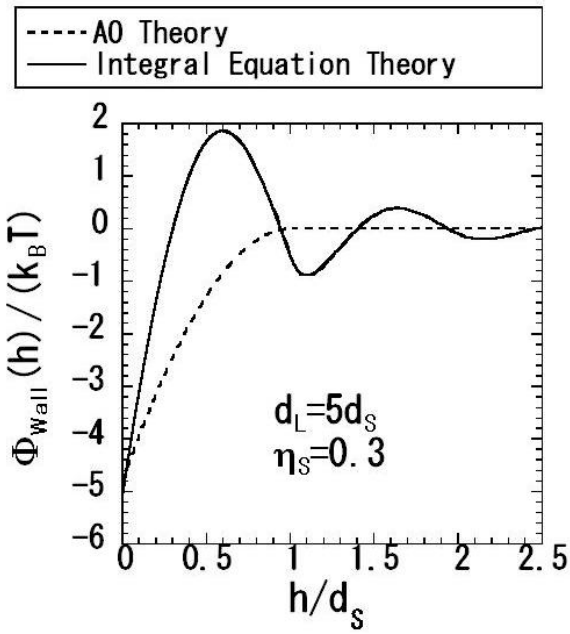

Figure 2. Entropic interaction Φ_{Wall} induced between a large sphere and a planar wall immersed in small spheres. T□k_B□h, d_L, and d_S denote the absolute temperature, Boltzmann constant, surface separation, diameter of the large sphere, and diameter of the small spheres, respectively. The results calculated using the Asakura-Oosawa (AO) theory and integral equation theory are compared.

purely entropic in origin), it is called the *entropic interaction*. The existence of the entropic interaction was first pointed out by Asakura and Oosawa (AO) (1, 2).

The presence of a planar wall in small spheres also generates an excluded volume. If a large sphere with diameter d_L contacts the wall in small spheres with diameter d_S (d_L>>d_S) as shown in Figure 1(b), the free energy of the small spheres changes by ΔF. Let us estimate ΔF within the framework of the AO theory (1, 2). The formula of the ideal-gas entropy,

$$S=k_B N_S \ln(V/N_S)+C=S(V), \quad (1)$$

is applied to the small spheres. Here, k_B is the Boltzmann constant, N_S the total number of small spheres in the system, V the total volume available to the translational motion of small spheres, and C a constant which is independent of V. The entropy change occurring upon the change "$V \rightarrow V+\Delta V$" ($\Delta V/V$<<1) is given by

$$\Delta S=S(V+\Delta V)-S(V)\sim k_B N_S \Delta V/V. \quad (2)$$

Expressing the overlapped volume ΔV (shadowed in Figure 1(b)) in terms of d_L and d_S and substituting the resultant expression into Equation (2) yields

$$\Delta F=-T\Delta S\sim -3k_B T\eta_S(d_L/d_S), \quad (3a)$$
$$\eta_S=\pi(N_S/V)d_S^3/6, \quad (3b)$$

where T is the absolute temperature. The free-energy gain becomes larger as the packing fraction of small spheres η_S increases and/or d_S decreases. It can be shown in a similar manner that the free-energy gain occurring when a pair of large spheres contact each other is $\sim -1.5k_B T\eta_S(d_L/d_S)$.

3.2. Effect of microstructure of small particles formed near large particles or a large particle and a planar wall

We concentrate on the hard-body model in which the small and large particles are hard spheres and the wall is a hard wall with no soft potentials. The entropic interaction induced between large particles or between a large particle and the wall is described within the framework of the Asakura-Oosawa (AO) theory (1, 2) in Section 3.1. However, the description is valid only when the packing fraction of small particles η_S is sufficiently low. In cases where η_S is high, due to the microscopic structure of small particles formed within the domain confined by two large particles or by a large particle and the wall, the entropic interaction oscillates (i.e., attractive and repulsive regions appear alternately) with the periodicity d_S (3-8). This effect can be accounted for only by employing elaborate statistical-mechanical theories such as the integral equation theory with the hypernetted-chain (HNC) or reference HNC (RHNC) closure for liquid states (9). (The Percus-Yevick (PY) closure gives a pathological density profile of small particles, which becomes negative near a large particle or the wall, and the entropic interaction cannot be calculated. The PY closure gives good results only for a hard-sphere mixture with very low size asymmetry.)

Figure 2 shows an example of the entropic interaction induced between a large sphere and the wall immersed in small spheres (the entropic interaction between large spheres exhibits qualitatively the same behavior). The entropic interaction is described in terms of the potential of mean force (PMF) $\Phi_{Wall}(h)$ where h is the distance between the nearest surfaces of the large sphere and the wall. $\Phi_{Wall}(h_0)$ represents the free energy of small spheres in the case of $h=h_0$ *relative to* that in the case of $h\rightarrow\infty$. $F_{Wall}(h)=-d\Phi_{Wall}(h)/dh$, which is shown in Figure 3, is the entropic force (mean force). $F_{Wall}(h_0)$ represents the

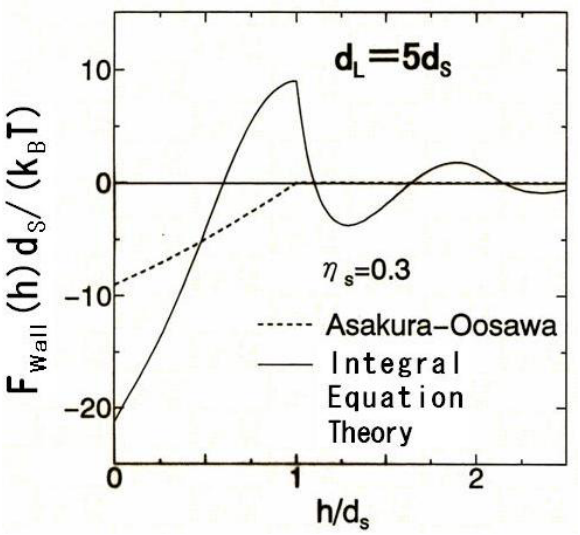

Figure 3. Entropic force F_{Wall} induced between a large sphere and a planar wall immersed in small spheres. T□k_{B}□h, d_{L}, and d_{S} denote the absolute temperature, Boltzmann constant, surface separation, diameter of the large sphere, and diameter of the small spheres, respectively. The results calculated using the Asakura-Oosawa (AO) theory and integral equation theory are compared.

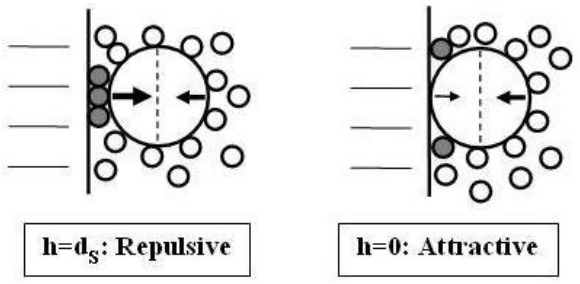

Figure 4. Left: Cartoon illustrating that the net force is repulsive at h=d_{S}. Right: Cartoon illustrating that the net force is attractive at h=0. h and d_{S} denote the surface separation and diameter of the small spheres, respectively.

force induced between the large sphere and the wall averaged over all possible configurations of the small spheres with h fixed at h_0. In Figures 2 and 3, two curves calculated using the integral equation theory and the AO theory are compared.

As observed in Figure 3, in the AO theory no force is induced between a large sphere and the wall as long as there is no overlap of the two excluded volumes generated. The overlap occurs only for h<d_{S} and a force is induced to increase the overlapped volume. The AO force is always attractive and its strength increases monotonically with decreasing h. By contrast, the *exact* force is oscillatory and longer-ranged. The reason for this is the following. The presence of a small sphere also generates an excluded volume for the other small spheres. As a consequence, the small spheres tend to be driven to contact the large sphere and the wall. This effect is often referred to as the *packing force*. A channel or corners can be formed by the large sphere and the wall as illustrated in Figure 4. The small spheres within the channel shown in the left cartoon and those at the corners shown in the right cartoon (those small spheres are marked in gray in the figure) contact both of the large-sphere and wall surfaces. Hence, contact densities of small spheres within the channel and at the corners become considerably higher (6, 7). As observed in the right cartoon, for h<d_{S} no small spheres can enter the channel. Due to these effects, a microstructure (i.e., the inhomogeneity of the contact density) of small spheres is formed within the confined domain. The thermal pressure acting on the large-sphere surface due to the small spheres becomes inhomogeneous, inducing a force between the large sphere and the wall (6, 7). In the left cartoon, for example, the channel is closely packed by the small spheres, causing higher thermal pressure. It follows that the force acting on the left side of large-sphere surface becomes stronger than that on the right side, and the net force is repulsive. In the right cartoon, on the other hand, in the left side there is a domain which no small spheres can enter, leading to zero thermal pressure. This effect dominates with the result that the force acting on the left side of large-sphere surface becomes weaker than that on the right side, and the net force is attractive.

As η_{S} decreases, the entropic interaction and force shown in Figures 2 and 3, respectively, become weaker and shorter-ranged, and the solid and broken curves approach each other. The two curves become completely indistinguishable at the limit $\eta_{\mathrm{S}}\rightarrow 0$. As described in Section 3.4, we consider *water* as the small spheres. For water at ambient temperature and pressure η_{S}=0.383 that is higher than the setting η_{S}=0.3 in Figures 2 and 3. In such cases, the two curves become even more different. Hereafter, we concentrate on the cases where η_{S} is as high as that for water.

We note that the two curves in Figure 2 share almost the same value of the PMF at contact $\Phi_{\mathrm{Wall}}(0)$. $\Phi_{\mathrm{Wall}}(0)$ is the free-energy gain ΔF of small spheres occurring when the large sphere contacts the wall. For simple cases such as large sphere-planar wall and large sphere-large sphere contacts, fortuitous cancellation of errors occurs in the calculation of $\Phi_{\mathrm{Wall}}(0)$ using the AO theory (6, 7). Equation (1), for example, remains fairly accurate up to η_{S}~0.4. (The AO theory sometimes fails in the estimation of the free-energy gain of small spheres, and an example case is described in Section 5.1). Only in the solid curve in Figure 2, however, there exists a free-energy barrier for the large sphere to overcome to contact the wall. In general, as the channel becomes wider, the repulsive peak observed in the solid curve in Figure 3 increases, leading to higher free-energy barrier. As discussed in Sections 3.6, 5.1, and 6.2, the height of the barrier often plays important roles. In any case, the entropic interaction is induced only when h becomes sufficiently short (only several times larger than d_{S}) and the effect of the microstructure of small spheres comes into play.

3.3. Effect of attractive potentials between small particles, a small particle and a large particle, or a small particle and a planar wall

If small particle-small particle, small particle-large particle, and small particle-planar wall potentials have attractive parts, the induced interaction between large particles or between a large particle and the wall becomes somewhat different (10). Regarding the hard-body system with no attractive parts as the reference system, we first discuss the case where the attractive part is present only between small particles (Case 1). Note that the coordination number for a small particle (i.e., the number of small particles which can contact a small particle) in contact with the large-particle or wall surface is roughly a half of that for a small particle in the bulk ("bulk" means the position which is far from the surface). Since the small particles interact though attractive potential, the energetic loss becomes larger as the number of small particles in contact with the surface increases. Therefore, the number density of small particles in the vicinity of the surface is driven to decrease, and this energetic effect competes with the packing force. The effect makes the induced interaction shift in a more attractive direction. For example, the contact shown in the right cartoon in Figure 4 is even more stabilized.

We then discuss the case where the attractive part is absent between small particles but it is present between a small particle and a large particle and between a small particle and the wall (Case 2). In this case the energetic gain becomes larger as the number of small particles in contact with the surface increases, leading to an upward shift of the induced interaction (i.e., the interaction shifts in a more repulsive direction). If the attractive part is quite strong, the contact shown in the right cartoon in Figure 4 is destabilized.

In a real system, the attractive part is present for all of the pairs, small particle-small particle, small particle-large particle, and small particle-planar wall. The effects in Cases 1 and 2 cancel each other to some extent, and if the attractive part between small particles is as strong as that between a small particle and a large particle and that between a small particle and the wall, the induced interaction can reasonably be described even by the hard-body model. We emphasize that the entropically induced interaction is omnipresent. It is quite strong if the packing fraction of small particles and the size asymmetry of small and large particles are high.

3.4. In real systems, what do small particles, large particles, and a planar wall, respectively, correspond to?

It is stated in Section 3.2 that the entropic interaction is induced between large particles only when they approach each other up to distances where the microstructure of small particles near the large particles becomes significant (i.e., only when the surface separation becomes smaller than several times of the diameter of small particles). In other words, if the large particles can approach each other up to such distances, the effect of the translational motion of small particles plays essential roles.

In the original argument made by Asakura and Oosawa (1, 2), the large particles and the small particles correspond to colloidal particles and polymers, respectively, and the solvent is treated as inert background. In the crowding concept (11, 12) developed by Minton and coworkers later, the large particles and the small particles correspond to larger biopolymers and smaller biopolymers (or molecules which are significantly smaller than biopolymers), respectively, and the solvent is treated in the same manner. However, these treatments are not valid except in the special system described below.

The special system is found in colloidal suspensions. The surface of a polystyrene particle has high negative charge density. Polystyrene particles immersed in pure water cannot approach each other up to a distance where the microscopic structure of water molecules near the particles comes into play, due to the strongly repulsive electrostatic interaction (the interaction is expressed as $Q_L^2/(\varepsilon r)$ where Q_L is the total charge of a particle, ε the dielectric constant of water, and r the distance between centers of two particles). If salt such as NaCl is added, the charge of the particle is screened by the counter ions Na^+. When the salt concentration is sufficiently high, the screening effect is strong enough to make the interaction between polystyrene particles much shorter-ranged, and the interaction at small r is influenced by the microstructure of water molecules and ions within the domain confined by two particles. However, if the salt concentration is too high (the threshold concentration is dependent on the surface charge density, but roughly beyond 0.5M), the effect arising from particle-counter ion electrostatic interaction predominates over the entropically induced interaction. On the other hand, at appropriate salt concentrations (~0.01M in the case of NaCl), the interaction between particles changes steeply near $h=\xi$ (h is the distance between the nearest surfaces of particles and ξ the Debye length). The interaction is essentially zero for $h>\xi$ while it is quite strong due to the electrostatic repulsion for $h<\xi$. Moreover, ξ is much larger than the molecular diameter of water, and the particles cannot approach each other up to a distance where the interaction is influenced by the microscopic structure of water molecules and ions near the particles. Therefore, the presence of the salt solution need not explicitly be considered, and the particle interaction can be approximated by a hard-sphere potential where the effective diameter of the hard spheres is "$d_P+\xi$" (d_P is the diameter of the polystyrene particles and $\xi<<d_P$). For a system comprising two species of particles different in size, the smaller particles form *small particles* and the larger particles correspond to *large particles*, and all of the particles are essentially hard spheres. The salt solution can be regarded as inert background. If a glass wall with negatively charged surface is also present, we can take the view that the system consists of large hard spheres and a hard wall immersed in small hard spheres. This type of system has been of considerable interest because it is best suited to the exclusive investigation of the entropic interaction in experiments (14-17), and quantitatively good agreement between the theoretical result and the

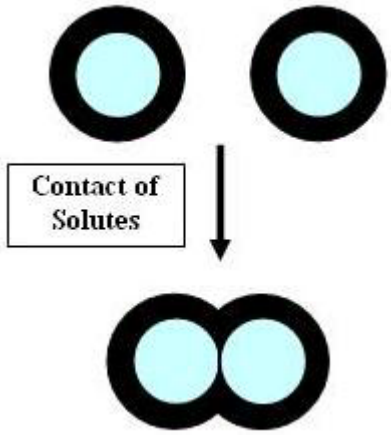

Figure 5. Contact of solutes immersed in solvent. The layer of solvent molecules whose structure differs from the structure of bulk solvent is shown in black, though the interface between the layer and the bulk is much less sharper than this figure shows.

experimental observation has been verified as mentioned in Section 3.7.

It seems that the solvent has been regarded as inert background in biological systems as a straightforward extension of the special system in colloidal suspensions described above. However, biopolymers are quite different from polystyrene particles in the following respects. A biopolymer consists of atoms or groups possessing negative and positive charges in various magnitudes. Since the salt concentration is relatively higher (~0.15M), the electrostatic interactions between charged groups are considerably screened. Moreover, the biopolymer has many nonpolar groups. Biopolymers or their portions can approach one another up to distances where the microstructure of water molecules and ions is of vital importance. When the entropic interaction between biopolymers or their portions is analyzed, it is not justified to treat the solvent as inert background. The primary component of the solvent is water: In biological systems, biopolymers corresponding to *large particles* are immersed in *small particles* of water molecules, and the membrane corresponds to *a wall*. As discussed in 7.2, molecular species whose sizes are smaller than those of biopolymers but larger than the size of water molecules correspond to *medium-size particles*. The major objective of the present review is to show the crucial importance of the translational motion of water molecules in biological systems.

3.5. Isochoric (constant-volume) and isobaric (constant-pressure) processes

In a strict sense the description in Section 3.1 is given for the isochoric process in which the system volume is kept constant before and after the contact of large particles occurs. We raise the following questions: How does the behavior change if the contact occurs in the isobaric process where the system pressure is kept constant?; and how are the effects of attractive parts included in the particle-particle potentials?

The free-energy gain of the solvent occurring upon the contact of solutes equals

"Solvation free energy of two solutes in contact with each other" –
"Solvation free energy of a single solute"×2. (4)

The solutes and solvent molecules correspond to the large particles and small particles, respectively. The solvation free energy is the excess chemical potential and the same in the isochoric and isobaric processes, whereas the solvation energy and entropy are not.

As illustrated in Figure 5, a layer of solvent molecules, within which the number density of solvent molecules differs from the bulk density, is formed around a solute. When two solutes contact each other, the total amount of the solute-induced layers (i.e., the total number of solvent molecules forming the layers) decreases. This is an important point to be emphasized (18). First, we consider the hard-body model where all of the solvent molecules and solutes are hard spheres. In this model system, the layers shown in Figure 5 have a density which is higher than the bulk density due to the packing force. If the contact of two solutes occurs *in the isochoric process*, the decrease in the excluded volume arising from the contact leads directly to the increase in the total volume available to the translational motion of solvent molecules: The entropic gain of the solvent is equivalent to its free-energy gain (whenever we refer to a gain or loss of entropy, we consider the entropy change multiplied by the absolute temperature). One might think that the decrease in the system pressure, which corresponds to the decrease in the excluded volume, occurs upon the solute contact. However, the pressure remains almost unchanged or decreases only slightly, because some of the solvent molecules which formed the enriched layers are released to the bulk. Even *in the isobaric process*, the system volume remains almost unchanged or it is slightly compressed. Due to the work done by the external system (the work cannot be neglected because the pressure of hard-sphere solvent is very high), part of the entropic gain which should occur in the isochoric process is converted to a corresponding enthalpic gain. The free-energy gain is the same in the isochoric and isobaric processes. Thus, the translational motion of solvent molecules in the isobaric process is as powerful as in the isochoric process as a force which drives the solutes to contact. We note that the contact of two solutes which have *already* been inserted into solvent is substantially different from the solute insertion into solvent. In the former, the pressure change in the isochoric process is much smaller.

Hereafter, we assume that the solvent molecules interact through strongly attractive potential like water molecules. Based on the results of our analyses (18) using the integral equation theory, we discuss the changes of excess thermodynamic quantities of the solvent upon the solute contact. When the attractive interaction potential for the solute-solvent pair is much weaker than that for the solvent-solvent pair, the solute is *solvophobic*. When the attractive interaction potential for the solute-solvent pair is

much stronger than that for the solvent-solvent pair, the solute is *solvophilic*. The free-energy change is the same in the isochoric and isobaric processes, but its distribution to the energy and entropy changes in the isobaric process differs largely from that in the isochoric process. Since the pressure is quite low (~1 atm) due to the strongly attractive solvent-solvent potential, the energy change almost equals the enthalpy change in the isobaric process. In what follows the solvent can be regarded as water. The solute contact generally accompanies an energy change and an entropic loss for the solutes themselves, but this effect is not included in the changes of excess thermodynamic quantities of the solvent.

First, the isochoric process is considered. Let ΔV_{ex} be "excluded volume generated by a pair of solutes in contact with each other" minus "excluded volume generated by a single solute"×2. The total volume available to the translational motion of solvent molecules changes by $-\Delta V_{ex}$ that is always positive.

1. Contact of solvophobic solutes in isochoric process: The contact accompanies an energy gain (i.e., energy lowering), entropic gain (i.e., increase in entropy), and free-energy gain (i.e., free-energy lowering) of the solvent. Since the solute-solvent contact is energetically unfavorable, the solute contact leading to a decrease in the solvent-accessible surface area gives an energy gain. A depleted layer, within which the density of solvent molecules is lower than the bulk density, is formed around a solute when the solute is highly solvophobic (see Appendix A): The total amount of the solute-induced layer decreases upon the solute contact (see Figure 5), leading to a lower pressure.

2. Contact of solvophilic solutes in isochoric process: The contact accompanies an energy loss, entropic gain, and free-energy loss of the solvent. The free-energy loss is due to the energy loss. An enriched layer, within which the density of solvent molecules is higher than the bulk density, is formed around a solute. Upon the solute contact some of the solvent molecules which formed the enriched, denser layers are released to the bulk. This effect dominates and the pressure becomes higher upon the solute contact.

In Case (2) if there is a solute-solute energy gain which overcomes the free-energy loss of the solvent plus the solute-solute entropy loss, the excess free energy of the whole system becomes lower upon the solute contact. We emphasize that the solute contact always gives an entropic gain of the solvent regardless of the solute solvophobicity or solvophilicity. The entropic gain is a major factor promoting the solute contact.

We then consider the isobaric process. Let ΔV_P be "partial molar volume of a pair of solutes in contact with each other" minus "partial molar volume of a single solute"×2. The total volume available to the translational motion of solvent molecules changes by "$-\Delta V_{ex}+\Delta V_P$". This change is usually positive, but it can be negative when the solute solvophobicity is quite high. The temperature is assumed to be higher than 277 K. (The behavior in cases where the temperature is lower than 277 K is summarized in Appendix B with our physical interpretation.)

3. Contact of solvophobic solutes in isobaric process: *When Case (1) is regarded as the reference*, a system-volume compression occurs with the result that the energy gain becomes larger while the entropic gain smaller. (When the solvent molecules interact through attractive potential, the volume compression and expansion usually cause an energy gain and loss, respectively.) If the solute solvophobicity is quite high, the solvent entropy can become lower upon the solute contact.

4. Contact of solvophilic solutes in isobaric process: *When Case (2) is regarded as the reference*, a system-volume expansion occurs and both of the energy loss and entropic gain become larger.

Even in Case (3) the free-energy lowering is the same as that in Case (1), and the translational motion of solvent molecules is always a major driving force of the solute contact. In Case (3) we can take the view that part of the entropic gain occurring in Case (1) is converted to a corresponding enthalpic gain. The quantity converted is dependent on T as described below. In Section 3.1, the expression, "the contact of large particles leads to a lower free-energy of small particles", is more appropriate than the expression, "the contact of large particles leads to a higher entropy of small particles", because the former covers both of the isochoric and isobaric processes.

Denoting the changes in the free energy, energy in the isochoric process, entropy in the isochoric process, energy in the isobaric process, entropy in the isobaric process, enthalpy, and system volume in the isobaric process upon the solute contact by $\Delta\mu$, ΔU_V, ΔS_V, ΔU_P, ΔS_P, ΔH, and ΔV_P, respectively, we can show the following equations (18):

$$\Delta H/(k_BT)=\Delta U_V/(k_BT)+(\alpha^*/\kappa_T^*)\Delta V_P/d_S^3, \quad (5a)$$
$$\Delta H=\Delta U_P+P\Delta V_P\sim\Delta U_P, \quad (5b)$$
$$\Delta S_P/k_B=\Delta S_V/k_B+(\alpha^*/\kappa_T^*)\Delta V_P/d_S^3, \quad (6)$$
$$\alpha^*=\alpha T, \quad (7a)$$
$$\kappa_T^*=\kappa_T k_BT/d_S^3, \quad (7b)$$
$$\kappa_T>0, \quad (7c)$$
$$\Delta\mu/(k_BT)=\Delta U_V/(k_BT)-\Delta S_V/k_B=\Delta H/(k_BT)-\Delta S_P/k_B. \quad (8)$$

Here, α is the isobaric thermal expansion coefficient, κ_T the isothermal compressibility, P the pressure, and d_S the diameter of solvent molecules. At P=1 atm, ΔH is almost equal to ΔU_P. In Case (3) $\Delta V_P<0$ and in Case (4) $\Delta V_P>0$. Water possesses the feature that $|\alpha|$ is extremely small below ~283 K (below 277 K $\alpha<0$ at 277 K $\alpha=0$ and above 277 K $\alpha>0$). Under this condition $|\alpha^*/\kappa_T^*|$ is negligibly small and the energy and entropy changes are almost the same in the isochoric and isobaric processes unless $|\Delta V_P|$ is quite large. Above ~283 K α^*/κ_T^* increases monotonically as T becomes higher. (The values of α^*/κ_T^* for water (d_S=0.28 nm) at some representative temperatures are as follows: –0.208 at 273 K, 0.052 at 278 K, 0.288 at 283 K, 0.894 at 298 K, 1.65 at 323 K, 2.14 at 348 K, 2.43 at 373 K.) The experimental data measured in the isochoric process expresses the effect of the translational motion of solvent molecules *more explicitly*

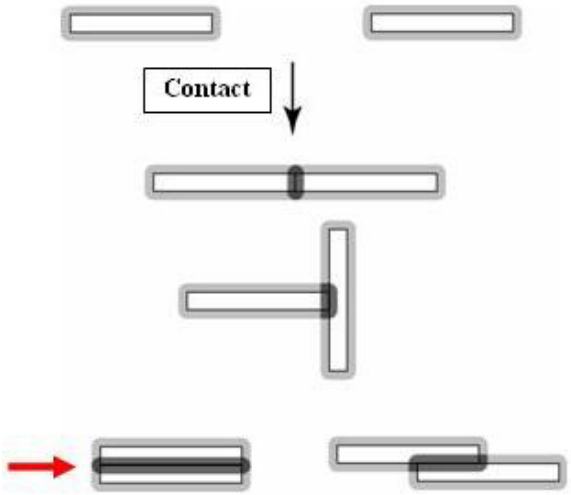

Figure 6. Four typical manners of contact of large particles immersed in small spheres. The large particles are long cylinders or thin discs. The small spheres are omitted here. The manner indicated by the red arrow leads to the largest reduction of the excluded volume.

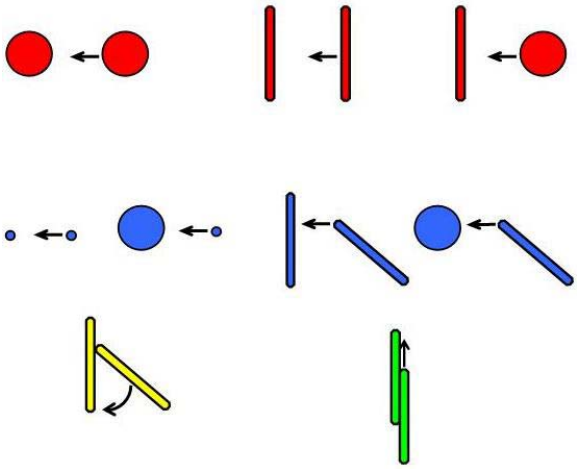

Figure 7. Some representative manners of approaching for large particles. As the large particles, "smaller sphere", "larger sphere", "long cylinder", and "thin disc" are considered. The small spheres are omitted here. It is assumed that the diameter of the smaller sphere is only a few times larger than the diameter of the small spheres d_S. The diameter of cross section of the cylinder and the thickness of the disc are also only a few times larger than d_S. The free-energy barrier is high in the manners shown in red, low in those in blue, very low in the sliding shown in green, and there is no barrier in the rotation shown in yellow.

than in the isobaric process in the sense that the entropic gain arising from the solute contact is preserved in its original quantity. The real experiments are performed in the isobaric process, but if T is sufficiently low, the data is close to that which could be obtained in the isochoric process.

The so-called enthalpy-entropy compensation (19-22), which means that the free-energy change is dependent on T only moderately though the entropy and enthalpy changes are strongly dependent, has been observed in a variety of physicochemical processes in aqueous environments. According to our theoretical results (18), as T becomes higher in Cases (1) and (2), $|\Delta U_V/(k_BT)|$ decreases whereas $\Delta S_V/k_B$ increases. They are somewhat compensating regardless of the solute solvophobicity or solvophilicity. This result is reasonable because the increase in thermal energy leads to a smaller effect of the interaction potential but to a larger entropic effect. As T becomes higher, $|\Delta V_P|$ decreases but beyond ~283 K $|(\alpha^*/\kappa_T^*)\Delta V_P/d_S^3|$ usually increases, and this effect can be dominant: In the case of $\Delta V_P<0$, ΔH and ΔS_P decrease with increasing T, while the opposite is true in the case of $\Delta V_P>0$ (see Equations (5) and (6)). The energy and entropy changes for water depend on T more strongly in the isobaric process than in the isochoric process, which comes from the presence of the term, $(\alpha^*/\kappa_T^*)\Delta V_P/d_S^3$. However, this term is cancelled out when the energy change, which is almost equal to the enthalpy change, is added to the entropy change to obtain the free-energy change. This feature enhances the compensation mentioned above for the isochoric process. The enthalpy-entropy compensation experimentally observed can thus be understood.

3.6. Cases where the asphericity of large particles is quite high

When the shape of large particles is highly aspherical (e.g., long cylinders, thin discs, etc.), the behavior of the entropic interaction is very interesting. For example, among the four contact manners of large particles shown in Figure 6, the contact indicated by the red arrow maximizes the volume of overlapped space (the space shadowed) and the free-energy gain of small spheres. Hence, the small spheres force the large particles to contact each other in the most regular manner. The effect of the translational motion of small spheres drives the large particles to form highly ordered structure.

The entropic interaction induced between large particles is dependent on their orientations and the distance between their centers. Here, we consider the entropic interaction for a special trajectory (or a special manner of approaching). We describe some of our theoretical results (23) with the emphasis on the free-energy barrier in the interaction. As illustrated in Figure 7, we consider "smaller sphere", "larger sphere", "long cylinder", and "thin disc" as the large particles in some representative manners of approaching. As described in Section 3.2, the free-energy barrier increases as the channel confined between two large-particle surfaces becomes wider. It is assumed that the diameter of the smaller sphere is only a few times larger than the diameter of small spheres d_S. The diameter of cross section of the cylinder and the thickness of the disc are also only a few times larger than d_S. Our conclusion is as follows: The barriers in the three interactions shown in red are high, those in the four interactions shown in blue are low, and those in the rotation and the sliding shown in yellow and in green, respectively, are zero or negligibly low. The reason why there is no barrier in the rotation is

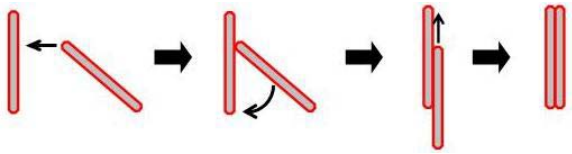

Figure 8. A possible manner in which long cylinders or thin discs reach the most stable contact.

described in detail in our earlier publication (23). It is difficult for very large spheres to reach the contact due to the high barrier. However, if at least one of the large particles has sufficiently high asphericity, as illustrated in Figure 8, they are capable of reaching the most stable contact by choosing particular manners of approaching. This interesting result becomes crucially important in Section 6.2.

The effect described in Sections 3.1 through 3.6, "regular or orderly contacts or aggregation of large particles are driven by the translational motion of small spheres", is referred to as the *entropic excluded-volume effect* or the effect of the translational motion of small spheres. The overall shapes and/or the detailed polyatomic structures of the large particles are essential in arguing this effect. The translational motion of large particles, which is also important, favors the dispersion of large particles in small spheres. This is the effect of entropy of mixing which competes with the excluded-volume effect. If the concentration of large particles is low, the former dominates. If it becomes sufficiently high, the latter becomes substantially larger.

3.7. Experimental evidence of entropic excluded-volume effect

Entropically driven phase separations have experimentally been observed for the special system in colloidal suspensions described in Section 3.4. Continually adding larger colloidal particles (corresponding to large particles) to smaller colloidal particles (corresponding to small particles) in suspension eventually leads to a separation into a crystal phase of larger particles (smaller particles are in the interstices if the diameter ratio is sufficiently small) and a fluid phase comprising mainly of smaller particles (14). When a glass wall is also present, the continual addition of larger particles results in the appearance of the crystal phase of larger particles on the wall surface at a concentration of larger particles that is significantly lower than in the absence of the wall (14, 15). In these experiments, it has been verified that the phase diagram is almost independent of the temperature, which shows that the potential between colloidal particles and between a colloidal particle and the wall can be approximated by the hard-body potentials (the Debye length is weakly dependent on the temperature but the effective diameters of the colloidal particles remain almost unchanged because of $\xi << d_P$; see Section 3.4).

The entropic interaction between larger colloidal particles introduced to smaller colloidal particles in suspension has also been measured as a function of the packing fraction of smaller particles (17). When the packing fraction is sufficiently low, the interaction is well described by the Asakura-Oosawa (AO) theory (1, 2). As the packing fraction increases, however, the transition from the monotonic curve to the oscillatory behavior (see Section 3.2) occurs, which necessitates the use of more elaborate statistical-mechanical theories such as the density functional theory (5, 8) and the integral equation theory. Regardless of the packing fraction, the theoretically calculated curve has been shown to be in *quantitatively* good agreement with the experimental observation.

3.8. Comments on "hydrophobicity"

A conventional view of the solute hydrophobicity, which is widespread in the protein research community, is based on the *iceberg* hypothesis. According to the iceberg picture, the structure of water around a nonpolar solute is much more ordered than in the bulk by strengthening hydrogen bonds or by an increase in the number of hydrogen bonds. The ordered structure is energetically stable but entropically unstable. The entropic instability predominates over the energetic stability with the result that the ordered structure is unstable in its free energy. To reduce the total amount of water forming the ordered structure, nonpolar solutes are driven to contact each other.

Our recent study (24) using the angle-dependent integral equation theory (24-32) for molecular liquids has suggested different molecular mechanisms of the hydrophobic effect. Upon the solute insertion, the translational and rotational motions of water molecules are restricted. However, the translational restriction contributes to the solvation free energy (SFE) much more than the rotational restriction. This trend becomes more appreciable as the solute size increases. The translational contribution can be described even by a model simple fluid in which the particles interact through strongly attractive potential like water and the particle size is as small as that of water. In fact, the presence of the minimum value of the solute solubility, which is widely believed to be a unique nature of the hydrophobic effect, can be reproduced using the simple-fluid model. The contribution from the solute-water translational correlation is larger than that from the solute-water orientational correlation for the solvation energy and entropy as well, particularly in the isochoric process. The water structure around the solute is not significantly different from the bulk water structure. The formation of highly ordered structure arising from the enhanced hydrogen bonding does not occur, or the enhancement is not strong enough to make a significant contribution to the SFE or the hydrophobic effect. It is concluded that the hydrophobic effect is ascribed to the interplay of the exceptionally small molecular size and the strongly attractive interaction of water, and not necessarily to its hydrogen-bonding properties.

The absence of highly ordered water structure around a nonpolar solute is supported by the results of computer simulations (19, 33) and neutron scattering experiments (19, 34). The new picture of the hydrophobicity mentioned above is consistent with the great success of the scaled particle theory (35) where water is treated as a simple fluid. Soda (36) has pointed out that the iceberg hypothesis contradicts the temperature

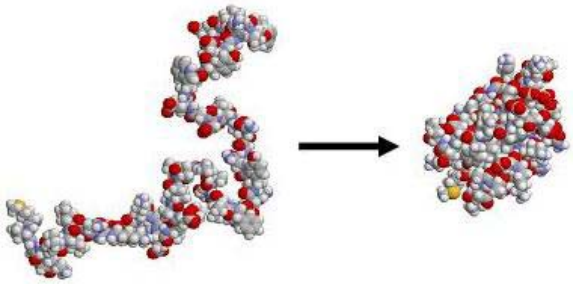

Figure 9. Illustration of protein folding. Oxygen, carbon, nitrogen, hydrogen, and sulfur atoms are shown in red, gray, blue, white, and yellow, respectively.

dependence of the thermodynamic quantities of hydrophobic hydration experimentally measured. Thus, many of the characteristics of the hydrophobic effect are not ascribed to the hydrogen-bonding network, rotational motion of molecules, and solute-water orientational correlations. The translational motion of water molecules is usually much more important, and its effects can be elucidated even by a simple fluid suitably modeled.

An important point is that when two large hydrophobic solutes contact each other, the total volume available to the translational motion of *the water molecules which are present in the system* increases, leading to a free-energy gain of water. As a notable example, pressure denaturation of proteins described in Section 4.8 can be elucidated not by the conventional view looking only at *the water structure in the vicinity of the protein* but by this new concept.

Here, it is worthwhile to emphasize the usefulness of the angle-dependent integral equation theory (24-32). In this theory the potential and correlations between molecules are explicitly treated as functions of their orientations as well as the distance between their centers. This is in contrast with the reference interaction site model (RISM) and related theories (37-39) in which the potential and correlations between molecules are represented by those between the interaction sites. In the RISM and related theories, the potential and correlations for a pair of interaction sites, which are dependent only on the distance between centers of the interaction sites, are treated separately from those for the other pairs *in the closure equation* (9). This treatment becomes problematic especially when the elucidation of the hydrophobic effect is undertaken. For example, the RISM and related theories give too high a value of the hydration free energy and wrong temperature dependence of the solute solubility (24). The angle-dependent integral equation theory is superior to them.

3.9. Ordering processes entropically driven

As seen in Equation (1), the entropic excluded-volume effect becomes larger for smaller d_S, higher η_S, and larger d_L. The molecular size of water is the smallest among the ordinary liquids in nature. The effect becomes the largest when the small spheres are water molecules. Though the molecular size of neon is about the same as that of water, it is in gas state at ambient temperature and pressure, resulting in a negligibly small effect. Cyclohexane is in liquid state but its molecular size is much larger than that of water, leading to a much smaller effect.

The biomolecules, which are immersed in water, are driven to form a variety of ordered structures and to exhibit highly advanced function for reducing the restriction for the translational motion of the water molecules which are present in the system. Self-assembling processes occur in order to increase the water entropy. These can be referred to as *entropically driven ordering processes*. As mentioned above, in the isobaric process part of the translational-entropy gain of water can be converted to a corresponding energy (or enthalpy) gain of water (18). In both of the isochoric and isobaric processes, the translational motion of water molecules is always a primary driving force. We give typical examples in the succeeding sections.

4. PROTEIN FOLDING

4.1. What is the major driving force in protein folding?

A protein, a long polypeptide chain, spontaneously folds into a unique native structure in aqueous solution under physiological conditions (see Figure 9). A feature common to the native structures of proteins is that the backbone and side chains are tightly packed and the interior contains little space (40). The tight packing in the interior is necessary to ensure that the native structure be stable and that partially denatured, inactive structures have negligible probability at ambient temperature. This means that protein folding undergoes a very large loss of the conformational entropy (CE) of a protein molecule. Then a question arises: "What is the principal factor competing with the CE loss in the folding?"

The prevailing view is that the water adjacent to a hydrophobic group is unstable especially in terms of the rotational entropy and the folding is driven by the release of such unfavorable water to the bulk through the burial of nonpolar side chains. We note, however, that a protein is characterized by the heterogeneity that hydrophobic and hydrophilic atoms and groups are rather irregularly distributed in the molecule (see Figure 9). Hence, the burial of nonpolar side chains is unavoidably accompanied by the burial of polar and charged groups. The database shows that when proteins fold, 83% of the nonpolar side chains, 82% of the peptide groups, 63% of the polar side chains, and 54% of the charged side chains are buried in the interior (40). Protein folding is in contrast to, for example, the aggregation of surfactant molecules as micelles where the nonpolar groups are almost completely buried while the charged groups are all exposed. The burial of nonpolar groups works much less effectively than one might expect. In fact, it has been suggested that the exposed area of the hydrophobic surface is not always correlated with the conformational stability of a protein (41) and that the polar group burial contributes more to the stability of the native structure than the nonpolar group burial (40). Thus, the burial of nonpolar groups is not powerful enough to compete with the CE loss

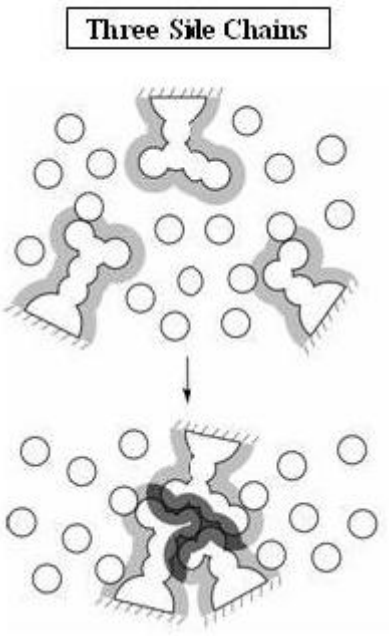

Figure 10. Close packing of side chains of a protein in aqueous solution.

The intramolecular energy gain is widely believed to be an essential factor driving a protein to fold: When a protein folds, very large stabilization occurs through a number of intramolecular hydrogen bonds formed and through van der Waals attractive interactions between protein atoms. As described in more detail in Section 4.4, however, the folding occurs in aqueous solution and accompanies serious *dehydration* penalty. The dehydration means the break of hydrogen bonds between water oxygen and protein oxygen or nitrogen (hereafter, this is referred to as "hydrogen bonds with water molecules") and the loss of van der Waals attractive interactions between protein atoms and water oxygen or hydrogen (or either of the break or the loss). It is quite doubtful that the intramolecular energy gain, which may accompany even a larger loss of the protein-water intermolecular energy, is a powerful driving force in the folding. There must be another powerful driving force which has been overlooked so far.

4.2. Statistical-mechanical analysis focused on the effect of translational motion of water molecules

We have analyzed the solvation free energy (SFE) of a protein molecule using the three-dimensional integral equation theory. The details of this theory are described in earlier publications (6, 42-44). The protein is modeled as fused hard spheres (the diameter of each hard sphere is set equal to the sigma-value of the Lennard-Jones potential assigned to the corresponding protein atom in AMBER 99) and immersed in hard spheres of diameter d_S=0.28nm (the diameter of water molecules) forming the solvent. Here, the SFE is the free-energy change upon the insertion of the protein molecule, whose structure is frozen, into a fixed point in the solvent. It is largely dependent on the structure. (When the solvent is water, it is often referred to as the hydration free energy.) Since there are no soft (Coulomb and van der Waals) interactions at all in this model system, all the allowed system configurations share the same energy and the system behavior is purely entropic in origin. Our analysis is focused on the effect of the translational motion of water molecules (43, 44). The SFE equals the negative of the solvation entropy multiplied by the absolute temperature. We note that the difference between two protein structures in the SFE cannot be calculated using the Asakura-Oosawa (AO) theory (1, 2) with sufficient accuracy because of the complex polyatomic structure of a protein molecule (43, 44).

It has been found for the C-peptide (the number of residues N is 13) that the SFE of the alpha-helix is lower than that of a random coil by $\sim 23k_BT$. That is, if the transition from the random coil to the alpha-helix occurs, the translational entropy of the solvent increases by $\sim 23k_B$, which corresponds to the free-energy gain of −14 kcal/mol at room temperature. Here, let us look at a real system. The free-energy change arising from the intramolecular hydrogen bonding *in water,* CO···W + NH···W → CO···HN + W···W (W denotes a water molecule), has been estimated to be 0±1 kcal/mol (45). Even if we assume that it is −1 kcal/mol, the total free-energy gain upon the alpha-helix formation of the C-peptide is only −9 kcal/mol because nine intramolecular hydrogen bonds are formed. Thus, the reduction of the restriction for the translational motion of water molecules is much more powerful as a driving force in the alpha-helix formation than the intramolecular hydrogen bonding.

The above result never suggests that the intramolecular hydrogen bonding is unimportant. It is imperative for compensating the serious penalty, the loss of hydrogen bonds with water molecules. The formation of the alpha-helix leads to a great reduction of the excluded volume for water molecules due to helical structure made by a portion of the backbone and contacts of side chains, and at the same time it ensures the intramolecular hydrogen bonds. We note that the formation of the helical structure by a long cylinder results in a great decrease in the excluded volume (7, 44, 46). Likewise, when the beta-sheet is formed, lateral contacts of portions of the backbone (see the lateral contacts of long cylinders shown in Figure 6) and contacts of side chains occur with ensuring the intramolecular hydrogen bonds. Thus, the alpha-helix and the beta-sheet are the most advantageous unit structures. It is no wonder that these two secondary structures frequently appear in the native structure of a protein.

Returning to the results of our model analysis, we discuss the folding of protein G (the number of residues N is 56). It has been found that the translational entropy of the solvent increases by $\sim 207k_B$ when protein G folds to its native structure from a random coil. When the side chains with a variety of geometric features are closely packed as illustrated in Figure 10, a reduction of the excluded volume occurring is much greater than in the contact of spherical particles shown in Figure 1(a). It is thus understandable that such a large entropic gain, $207k_B$, is reached upon the folding

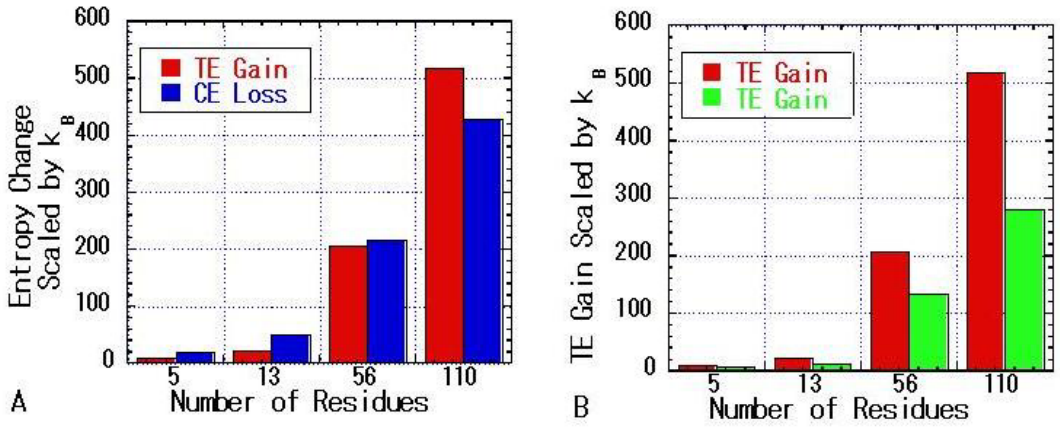

Figure 11. (a) Comparison between the conformational-entropy (CE) loss of the protein and the translational-entropy (TE) gain of water upon the folding for two peptides and proteins. For the smallest peptide, a compact structure stabilized in vacuum is used instead of the native structure. (b) Comparison between the TE gains in two cases: In the case shown in red the solvent diameter is equal to the molecular diameter of water, but in the case shown in green it is 1.5 times larger.

A great concern is to check if the translational entropy (TE) gain of the solvent upon folding is large enough to compete with the CE loss that is quite large. We have compared the TE gain of the solvent and the CE loss upon the folding from the random-coil state to the native state (i.e., a set of folded structures) (43, 44). Figure 11(a) shows the results for Met-enkephalin with N=5, the C-peptide with N=13, protein G with N=56, and barnase with N=110. Since Met-enkephalin takes an extended structure in aqueous solution, a compact structure stabilized in vacuum is used instead of the native structure. The CE of the random-coil state is roughly estimated as follows. For the backbone, per residue there are two dihedral angles which can rotate and each angle has three stable values. Therefore, the number of possible combinations is 3^2=9. The contribution from the backbone to the CE is set at $k_B\ln(9^N)$ for a polypeptide chain with N residues. Based on the computer simulation study by Doig and Sternberg (47), we regard the contribution from the side chain to the CE as $1.7k_B$ on an average per residue ($1.7Nk_B$ for a polypeptide chain with N residues). The CE of the native state is regarded as zero.

As observed from Figure 11(a), for the small peptides with N=5 and N=13 the TE gain is not powerful enough to compete with the CE loss, but for the proteins the TE gain and the CE loss share almost the same magnitude. This result is consistent with the well-known experimental evidence that small peptides do not fold and only sufficiently large peptides and proteins are foldable. If the solvent diameter was made 1.5 times larger than the molecular diameter of water with the packing fraction unchanged, the TE gain is no longer able to compete with the CE loss as observed in Figure 11(b). The exceptionally small size of water molecules is crucially important.

We have generated some different structures of protein G and compared them with the native structure, which has one alpha-helix and one beta-sheet as illustrated in Figure 12, in terms of the SFE (43, 44). Our findings are as follows. The SFE of a structure with the same alpha-helix but without the beta-sheet is higher than that of the native structure by ~$46k_BT$. As described above, the formation of the alpha-helix should lead to large stabilization. Nevertheless, a structure with four α-helices is less stable than the native structure in terms of the SFE by ~$33k_BT$. This result is indicative that the non-local intramolecular contacts as well as the local structures are quite important in the stabilization. A structure which is more spherical than the native structure gives the SFE which is higher by ~$76k_BT$. The tight packing specific to the amino-acid sequence of protein G gives rise to the slight asphericity of the native structure (see Figure 12).

For protein G, we have tested six hundred structures which were taken from local-minimum-energy structures in the trajectory of an exhaustive computer simulation using the all-atom potentials including Coulomb and Lennard-Jones (48). There are only several structures whose SFE is lower than that of the native structure (this is revisited in Section 4.4). We can conclude that the translational motion of solvent molecules plays critical roles in stabilizing the native structure. In other words, a protein tends to fold into a structure almost minimizing the restriction for the translational motion and maximizing the solvent entropy. A homopolymer takes extended structures when its monomer unit is hydrophilic, whereas it favors compact structures when it comprises hydrophobic monomers. A heteropolymer, which is characterized by its heterogeneity like a protein, does not possess a unique structure. A polypeptide chain with an arbitral amino-acid sequence does not possess a unique structure, either. A number of different structures can be stabilized in these examples. By contrast, a protein is capable of folding into a unique structure in which secondary structures are included and side chains with a variety of geometric features are characteristically locked. The amino-acid sequences which can realize this type of folding have been selected by nature. The geometric features (sizes, overall shapes, and details of the polyatomic structures) of side chains are prudently arranged in each sequence

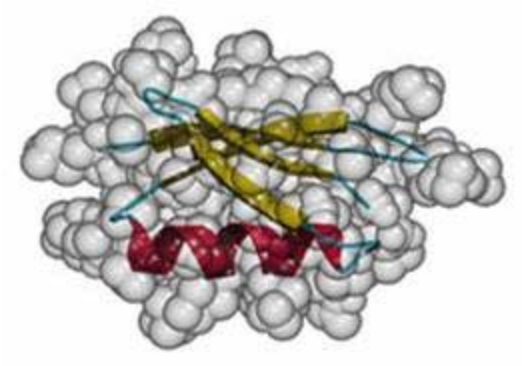

Figure 12. Native structure of protein G (PDB Code: 2GB1). It possesses one alpha-helix (marked in red) and one beta-sheet (marked in yellow).

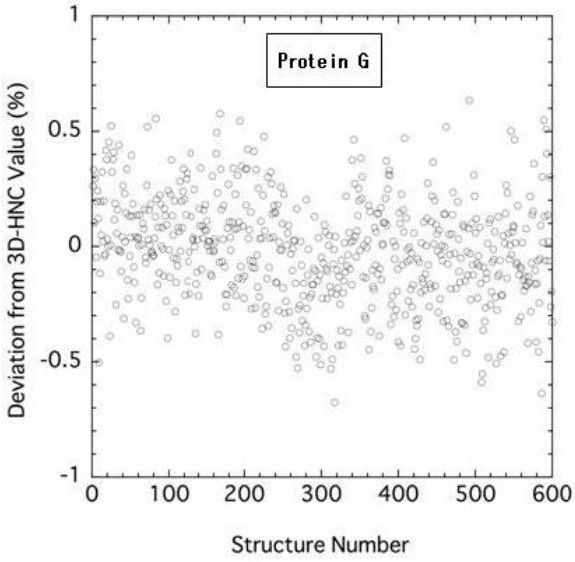

Figure 13. Discrepancy between the solvation free energy calculated using the three-dimensional integral equation theory with the hypernetted-chain (HNC) approximation and that using the morphometric approach (see Equation (10)). 600 structures of protein G are considered.

4.3. Morphometric approach to solvation thermodynamics of a protein

The solvation free energy (SFE) of a protein with a fixed structure is the key quantity in analyzing the solvent effects on the structural stability. However, the calculation of this quantity is a nontrivial task. The usual computer simulations can be applied only to small solutes. The three-dimensional version (6, 42) of the integral equation theory, which is employed in Section 4.2, is applicable to a large, complex solute molecule like a protein. However, it suffers a large computer memory and a long computation time required, and matters become quite serious when the SFE needs to be calculated for a number of different structures. We have developed a method based on morphometric thermodynamics (49) that allows us to calculate the SFE with sufficient accuracy in a computation time which is about four orders of magnitude shorter (50).

In the morphometric approach, the SFE μ is expressed using only four geometrical measures of a complex solute molecule like a protein with a fixed structure and corresponding thermodynamical coefficients. The expression is

$$\mu/(k_BT)=C_1V+C_2A+C_3X+C_4Y, \quad (9)$$

where V, A, X, and Y are the volume excluded by the protein, the surface area accessible to the solvent, and the integrated mean and Gaussian curvatures of the accessible surface, respectively. As the solute size becomes increasingly larger (i.e., at the large solute limit), the four coefficients (C_1, C_2, C_3, and C_4) multiplied by k_BT approach the pressure of the solvent, the surface tension of the solvent at a planar wall, and two bending rigidities which account for the curvature effects, respectively. The idea of the morphometric form expressed by Equation (9) is that it separates the geometric properties of the solute molecule and the four coefficients. This separation allows us to determine the four coefficients in simple geometries. They are determined from calculations of $\mu/(k_BT)$ for spherical solutes with various diameters followed by the application of the least square fitting. In principle the coefficients can be determined via any route: for example, the angle-dependent integral equation theory (24-32) combined the multipolar water model (25, 26) and a computer simulation using the SPC/E model (51) for water. The features of the model and theory are reflected in the coefficients. The value of $\mu/(k_BT)$ for a fixed structure of a protein is obtained only if the four geometric measures are calculated.

As the first step, we have calculated the SFE μ for the six hundred structures of protein G considered in Section 4.2 using the morphometric approach. As in Section 4.2, the protein is modeled as fused hard spheres and the solvent comprises hard spheres. The four coefficients are determined by employing the radial symmetric integral equation theory (9). Denoting the values of μ calculated using the three-dimensional integral equation theory and the morphometric approach by μ_I and μ_M, respectively, we define the discrepancy D(%) by

$$D=100(\mu_I-\mu_M)/\mu_I. \quad (10)$$

Figure 13 shows D plotted against the gyration radius R_g. The values of D are within ±0.7%. The computation time required in the morphometric approach is about four orders of magnitude shorter than in the integral equation theory. The computer memory required is also made far smaller. The calculation can readily be done even on a small personal computer. The computation time required per structure of protein G is less than 0.1 sec on the Itanium workstation. Even a very large protein or a protein aggregate can be handled without difficulty. This is a remarkable progress.

The morphometric form expressed by Equation (9) can be applied not only to the SFE but also to any thermodynamic quantity of solvation. We now consider the case where a hard-sphere solute is inserted into a model

water in the isochoric process (52). The angle-dependent integral equation theory, which is combined with the multipolar model of water, is employed. At ambient temperature and pressure, in the morphometric form applied to $\mu/(k_BT)$, $C_1>0$, $C_2>0$, and $C_1<<C_2$. When the form is applied to $U/(k_BT)$ and S/k_B, both of the values of C_1 are large and negative, but their absolute values are roughly the same with the result that C_1 for $\mu/(k_BT)=U/(k_BT)-S/k_B$ takes a very small, positive value. For the hard-sphere solvent, on the other hand, the solvation energy is zero: $U/(k_BT)=0$. In the form applied to $\mu/(k_BT)=-S/k_B$, C_1 takes a large, positive value but C_2 is negative. For $\mu/(k_BT)$ and $U/(k_BT)$, there is a great difference between water and hard-sphere solvent in terms of the properties of C_1 and C_2. However, the behavior of C_1 and C_2 in the form applied to S/k_B for water is qualitatively similar to that for hard-sphere solvent. This is why the effect of water entropy can roughly be analyzed by employing the hard-sphere model for water. Interestingly enough, when the form is applied to $\mu/(k_BT)$ for water at very high pressures, C_1 takes a large, positive value and C_2 is negative. That is, at very high pressures water behaves like hard-sphere solvent, probably because the elevated number density leads to the break of a number of hydrogen bonds and/or to the dominance of the repulsive parts of water-water potentials.

4.4. Energetics of protein folding

The function that plays the key role in analyzing the structural change of a protein, which we denote by W, is the sum of the protein intramolecular energy E_I and the hydration free energy μ: $W=E_I+\mu$. The hydration free energy is the same in the isobaric and isochoric processes. Therefore, we are free to choose the process and in the following we consider a structural change in the isochoric process. The hydration free energy consists of the hydration energy E_H and the hydration entropy S: $\mu=E_H-TS$ (T is the absolute temperature). The principal components of E_H are the energy gain of water arising from the compression of water caused by the protein insertion (component 1) and the protein-water interaction energy (component 2). Let ΔQ be the change in Q upon a structural change of a protein. We have the following equation:

$$\Delta W=\Delta E_I+\Delta\mu=\Delta E_I+\Delta E_H-T\Delta S. \quad (11)$$

Component 2 makes a dominant contribution to ΔE_H. When a protein changes its structure to a more compact one, for example, there is a gain in E_I (e.g., E_I becomes lower and $\Delta E_I<0$) due to the formation of intramolecular hydrogen bonds and van der Waals attractive interactions. At the same time, however, such a structural change accompanies the loss of protein-water interaction energy and E_H ($\Delta E_H>0$) becomes higher because the water-accessible surface area decreases. In general, the signs of ΔE_I and ΔE_H are opposite but their absolute values are comparable in magnitude.

We have proposed the concept that ΔE_I and ΔE_H are largely compensating (i.e., their magnitudes are not far from each other and their signs are opposite) (53). It has been verified by us for the native structure and a set of random coils of protein G using the three-dimensional reference interaction site model (3D-RISM) theory combined with the realistic all-atom model for the protein-water system (54). By "realistic" we mean that the atom-atom potential consists of Coulomb plus Lennard-Jones. According to our results, ΔE_I upon folding is quite large but greatly cancelled by almost equally large ΔE_H: $|(\Delta E_I+\Delta E_H)/\Delta E_I|$ upon folding is only ~0.060. "$\Delta E_I+\Delta E_H$" alone is not likely to be capable of competing with the conformational entropy loss. Thanks to the presence of the primary component of ΔW, $-T\Delta S$, ΔW can surpass the conformational entropy loss. (As argued in Sections 4.5 and 4.6, in general "$\Delta E_I+\Delta E_H$" takes a positive value.)

A great advantage of considering the structural change of a protein in terms of the hydration entropy S *in the isochoric process* is as follows. S is governed by the excluded-volume effect originating from the translational motion of water molecules and not greatly dependent on the protein-water interaction. We have considered the native structures of a total of eight peptides and proteins and calculated S using the 3D-RISM theory combined with the all-atom potentials (55). Even when the protein-water electrostatic potentials, which are quite strong, are shut off and only the Lennard-Jones potentials are retained, S decreases only by less than 5%. Further, an approximate value of S can be obtained even by employing a simplified model where the protein comprises a set of fused hard spheres and hard spheres form the solvent, as long as the solvent diameter and packing fraction are set at those of water. Suppose that we are to select the structure minimizing S from among a number of structures. If the structures are fairly different from one another, the selection can successfully be made by the simplified model described above. In a more sophisticated analysis treated in Section 4.6, however, the protein can still be modeled by fused hard spheres but a realistic molecular model must be adopted for water.

Hereafter, we calculate S using the morphometric approach (50). For the six hundred structures considered in Sections 4.2 and 4.3, we have calculated S and examined $\Lambda=-S-(-S)_{Native}$ (the subscript "Native" denotes the value of the native structure). $-S$ is positive and a smaller value of $-S$ implies a higher entropy of the solvent. Three models are tested for the solvent (53). In model 1, the solvent is treated as hard spheres with diameter d=0.28 nm. In this model $S=-\mu/T$. In model 2, spheres forming the solvent interact through strongly attractive pair potential $u(r)$ given by

$$u(r)=\infty \quad \text{for } r<d, \quad (12a)$$
$$u(r)=-\varepsilon(d/r)^6 \quad \text{for } r\geq d. \quad (12b)$$

The value of $\varepsilon/(k_BT)$ is chosen to be 1.8 for T=298 K. Model 3 is a much more realistic model of water. A solvent molecule is a hard sphere with diameter d in which a point dipole and a point quadrupole of tetrahedral symmetry are embedded (25, 26). The angle dependent integral equation theory (24-32) is employed to calculate the four coefficients in the morphometric form. In the theory the

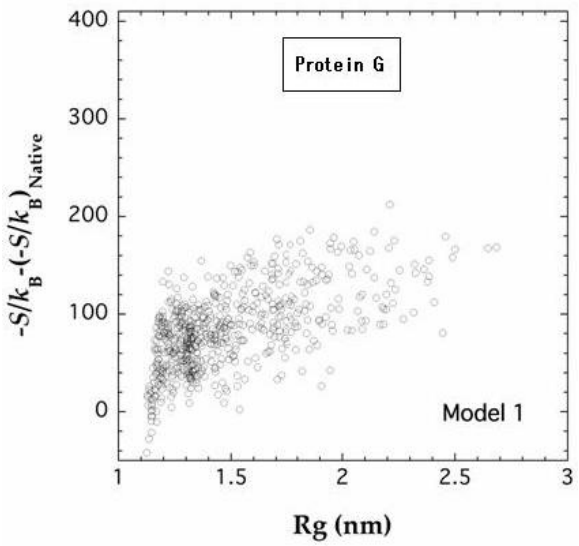

Figure 14. $F=-S-(-S)_{Native}$ plotted against gyration radius R_g. S is the hydration entropy in the isochoric process. The solvent is formed by hard spheres.

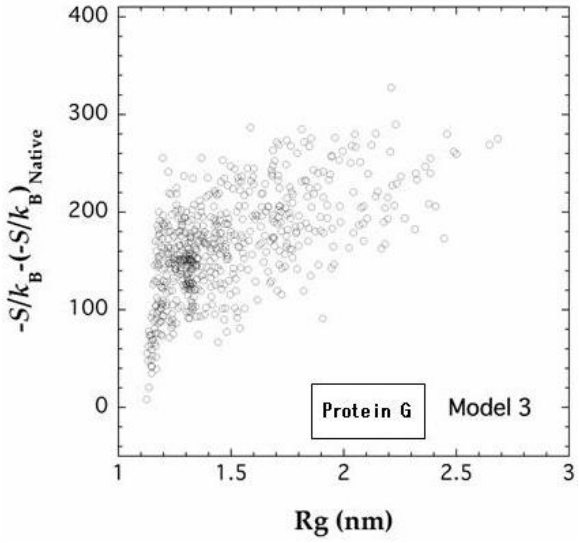

Figure 15. $F=-S-(-S)_{Native}$ plotted against gyration radius R_g. S is the hydration entropy in the isochoric process. The solvent is water represented by the multipolar model.

effects of the molecular polarizability are taken into account at a mean-field level.

Figures 14 and 15 show the plot of Λ for models 1 and 3, respectively, against the radius of gyration R_g. There is a general trend that Λ becomes smaller as R_g decreases. In model 1, there are several structures giving negative Λ. In models 2 and 3, on the other hand, there are no structure with negative Λ. That is, the solvent entropy takes the maximum value when the protein is in its native structure. It is interesting to note that the relative values of the solvent entropy among different structures are magnified when the solvent-solvent attractive interaction is incorporated. It can thus be suggested that the native structure can be characterized as the structure almost maximizing the entropy of water. The solvent-solvent attractive interaction has been shown to be important in evaluating the entropy. However, the details of water molecules such as the rotational motion appear to be insignificant and the structural stability of a protein can be analyzed using model 2. The above result is indicative that $-T\Delta S$ in Equation (11) plays a critical role in the structural stability of a protein as long as a suitable model is employed for water.

We note that if the four coefficients in the morphometric form are calculated using the RISM and related theories (37-39), even with a realistic water model such as the SPC/E (51) the difference between protein structures in S is considerably underestimated, and what is worse, several structures giving negative Λ appear (56).

Considering protein folding in the isochoric process, we can reach the following picture: A protein in aqueous solution under physiological conditions folds into the structure achieving the highest possible entropy of water under the requirement that as many intramolecular hydrogen bonds as possible be formed to compensate the dehydration penalty. In such a structure, many secondary structures are formed and the backbone and side chains with a variety of geometric features are closely packed, which leads to the uniqueness of the native structure and its high stability.

4.5. Relevance to experimental observations

Protein folding and aggregation are much more complicated than the contact of simple solutes treated in Section 3.5. There are two major points to be newly considered in these phenomena. Firstly, though the contact of hydrophobic groups may be dominant, the contacts of hydrophilic groups and those of hydrophobic and hydrophilic groups also take place (see Section 4.1). The effects of the system-volume compression and expansion are cancelled out to some extent in the isobaric process, and the behavior differs from that in the isochoric process much less than in cases of the contact of simple solutes (18). For example, protein folding in the isobaric process does not accompany the lowering of the water entropy mentioned for Case (3) in Section 3.5. Secondly, the gain of the protein intramolecular and protein-protein intermolecular energies and the loss of the conformational and translational entropies of protein molecules are included in the changes in the thermodynamic quantities experimentally observed. Moreover, the loss in the conformational entropy becomes larger with increasing temperature (see Section 4.9). Despite these differences, some of the theoretical results described in Section 3.5 can also be applied to protein folding and aggregation.

Here, we discuss protein folding. The experiments are usually performed for protein *unfolding* in the isobaric process. When the numerical data of the change in a thermodynamic quantity is simply multiplied by −1, the resultant value represents the data for protein *folding* discussed here. Since the enthalpy-entropy compensation occurs in the contacts of all groups, it is also observed for

protein folding (19). Judging from the results described in Section 3.5, we can conclude that the dehydration of a hydrophobic group upon the folding makes a negative contribution to the system-volume change while that of a hydrophilic group makes a positive contribution. The contribution from the dehydration of a hydrophobic group to the water-entropy change becomes smaller with increasing temperature whereas that of a hydrophilic group becomes larger. This argument is in qualitative accord with the result reported by Privalov *et al.* (57) who analyzed the experimental observations.

Since the burial of hydrophobic groups is dominant as compared to that of hydrophilic groups in protein folding, the system volume should decrease (ΔV_P<0). (We note that the system-volume decrease is much smaller than the decrease in the excluded volume generated by the protein upon the folding.) It follows that beyond 277 K part of the gain of the translational entropy of water, which should occur in the isochoric process, is converted to a corresponding enthalpic gain (see Section 6.2). If $|(\alpha^*/\kappa_T^*)\Delta V_P/d_S^3|$ is a monotonically increasing function of the temperature T beyond ~283 K as described in Section 3.5, as T increases the quantity converted becomes larger and eventually the observed entropy change (the sum of the water-entropy change and the negative conformational-entropy change) and enthalpy change (the sum of the water-enthalpy change and the negative intramolecular-energy change) become negative. The entropy and enthalpy changes decrease monotonically with increasing temperature. This interpretation does not contradict the experimental observations for protein folding (58-60). The temperature derivative of the enthalpy change is the change in the specific heat. The behavior that the enthalpy change decreases with increasing temperature is consistent with the experimental evidence that the change in the specific heat upon the folding is negative. The experimentally observed negative entropy change never denies the effect of the translational motion of water molecules as a driving force in protein folding. The experimentally observed negative enthalpy change is not necessarily indicative that the intramolecular-energy gain drives the protein to fold.

As discussed in Section 3.5, at 277 K the changes in thermodynamic quantities (entropy and enthalpy) of water upon protein folding in the isobaric process are the same as those in the isochoric process (at 1 atm the change in energy is almost equal to that in enthalpy). The conformational-entropy loss and intramolecular-energy gain are included in the experimentally measured entropy change and enthalpy change (these changes are both negative), respectively. According to the experimental results, the entropy and enthalpy changes are usually both positive at 277K (58-60). Even at 298 K there are significantly many proteins for which the changes are both positive (19). Very recently, Terazima (61) and coworkers have found using novel experimental techniques that the enthalpy change upon the folding of apoplastocyanin takes a very large, positive value in the temperature range 288–303 K (it exceeds 200 kcal/mol at 298 K). The entropy change, which must be positive, is even larger. A feature of the apoplastocyanin folding revealed in the experiment is that the system-volume change is almost zero: The folding takes place under constant-volume and constant-pressure conditions. The entropic gain, which arises from the reduction of the translational restriction for water molecules in the system, is completely reflected in the experimental data. The conversion of part of the entropic gain to a corresponding enthalpic gain does not occur. Their finding clearly indicates that the folding is driven by the water-entropy effect.

4.6. Construction of a novel method for predicting the native structure

Protein folding is the most fundamental and universal example of the biological self-assembly. The prediction of the native structure of a protein from its amino-acid sequence, which is one of the most enthusiastic subjects in modern science and technology, is an extremely difficult problem which has remained unresolved for these fifty years. It appears that a breakthrough is not likely to be obtained unless a unique concept, which is totally different from the conventional approaches, is employed. Many of the researchers employ the all-atom model for the protein-water system with the Coulomb plus Lennard-Jones potentials and explore the structural space using a computer (usually molecular dynamics) simulation. However, the huge amount of computational effort required has been a major stumbling block. Water is often treated as dielectric continuum, but the critical roles of water as a molecular ensemble cannot be taken into consideration. An even more serious problem is that the result obtained is strongly dependent on the force parameters employed (62). Hence, the techniques based on bioinformatics have been the most popular. The amino-acid sequence data base constructed for proteins whose native structures are known is investigated using the bioinformatics techniques and a set of candidate structures are generated. However, it is always a hard task to select the best structure. Further, such techniques suffer the drawback that the water effects are not taken into consideration and uncovering the folding mechanism is not undertaken. Here, we describe our novel method that has recently been developed (63).

In general, unlike the 600 structures of protein G treated in Sections 4.2–4.4, the structural stability of a protein cannot be argued simply in terms of the hydration entropy. This is particularly true for the structures generated by a bioinformatics technique which may include rather improbable (in terms of the intramolecular energy) structures. Hence, we consider a new free-energy function F which is crucially important in arguing the structural transition of a protein:

$$F=(-TS+\xi)/(k_B T_0),\ T_0=298\ \text{K}. \quad (13)$$

The hydration entropy S is calculated using the multipolar model (25, 26) for water and the angle-dependent integral equation theory (24-32) combined with the morphometric approach (50). ξ corresponds to the sum of the hydration energy (not free energy) and the intramolecular energy when the fully extended structure is chosen as the standard one with ξ=0. ξ is the total dehydration penalty

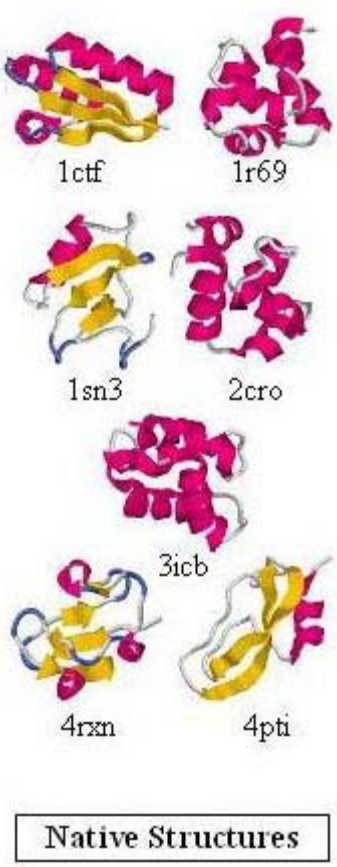

Figure 16. Seven proteins considered to test our energy function for discriminating the native fold from misfolded decoys. The alpha-helix is marked in red and the beta-sheet is marked in yellow.

accompanying a transition to a more compact structure. Compared to the fully extended structure which possesses the maximum number of hydrogen bonds with water molecules and no intramolecular hydrogen bonds, in a more compact structure some donors and acceptors (e.g., N and O, respectively) are buried in the interior after the break of hydrogen bonds with water molecules (CO···W□NH···W, etc.). There is no problem if the intramolecular hydrogen bonds (CO···HN, etc.) are formed. However, it is not always formed, leading to the dehydration penalty.

Hereafter, T is set at T_0. We consider the dehydration arising from the break of hydrogen bonds with water molecules alone by assuming that the gain of van der Waals attractive interactions between protein atoms is completely cancelled by the loss of van der Waals attractive interactions between protein atoms and water oxygen or hydrogen. According to the results from the computer simulation performed by Brooks *et al.* (64) for hydrogen-bond formation between two formamide molecules, the free-energy gain in the formation of CO···HN *in a nonpolar liquid* is about –8.4 kcal/mol at 298 K that is $\sim -14k_BT_0$ while that in water is only $-0.5k_BT_0$. Since the value, $-0.5k_BT_0$, is variable depending on the amide species and more or less uncertain (64, 65), we regard it as zero. The process considered by Brooks *et al.* does not quite correspond to the transition to a more compact structure for a protein. For example, what they calculate is not the energy gain we need but the free-energy gain. Pending further studies on the formation of CO···HN, we adopt the following method by choosing the fully extended structure as the standard one. When a donor and an acceptor are buried in the interior (it is assumed to have a nonpolar-liquid environment) after the break of hydrogen bonds with water molecules, if they form an intramolecular hydrogen bond, we impose no penalty. On the other hand, when a donor or an acceptor is buried with no intramolecular hydrogen bond formed, we impose the penalty of $7k_BT_0$ (this is one half of $14k_BT_0$).

We have to determine if each of the donors and acceptors is buried or not. The water-accessible surface area is calculated for each of them. If it is zero, the donor or acceptor is considered buried. That is, the dehydration penalty of $7k_BT_0$ is imposed only when the donor or acceptor is completely buried. We examine all donors and acceptors for backbone-backbone, backbone-side chain, and side chain-side chain intramolecular hydrogen bonds and calculate ξ. $-S$ and ξ, which are both positive, are functions of the protein structure, temperature, pressure, and so on.

In the protein research community, "decoy" sets (66) are prepared for a number of proteins so that people can check the power of their energy function. Each decoy set comprises the data of nearly one thousand *misfolded* structures. Most of them were generated using bioinformatics and related techniques. Structures which are similar to the native fold are included in the data set. The power of the energy function can be evaluated by checking if the native fold gives the lowest value of the energy function and it can thus be selected from among the decoy and native folds. If there is even one structure whose energy function is lower than that of the native fold, the energy function fails. In this sense, the introduction of ξ into Equation (13) is essential.

We have tested F given by Equation (13) as the energy function for decoy sets of seven proteins and succeeded in identifying the native fold as the structure with the lowest value of F (63). The seven proteins chosen are vitamin-B-dependent calcium binding protein (3icb), the amino terminal domain of 434 repressor (1r69), 434 Cro protein (2cro), the C-terminal domain of ribosomal protein (1ctf), scorpion neurotoxin (1sn3), trypsin inhibitor (4pti), and rubredoxin (4rxn). The numbers of residues of these proteins are in the range 54-76. The native folds of the seven proteins exhibit a great variation with alpha-helix and/or beta-sheet structures as shown in Figure 16. The decoy databases corresponding to these proteins contain 627-687 structures. In order to remove serious overlaps of protein atoms, the native and decoy structures are minimized either in vacuum in terms of the CHARMM energy (67, 68) or in water modeled as a dielectric continuum in terms of the CHARMM/GB energy (68). The computer programs, CHARMM (69) and MMSTB (70), are

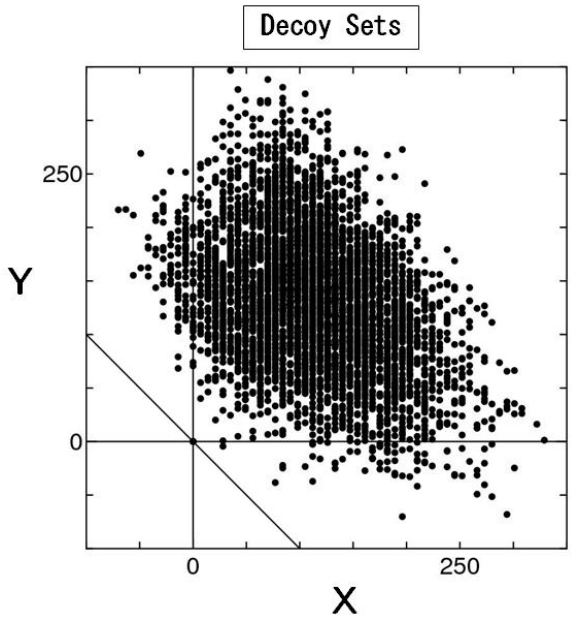

Figure 17. Relation between Y and X (see Equations 14-16). The data for all the seven proteins considered are collected. The three lines drawn represent X=0, Y=0, and X+Y=0, respectively.

used for the minimization. The CHARMM energy is the intramolecular potential energy of a protein, and in the CHARMM/GB energy water effects are additionally taken into consideration. After the minimization, each structure is switched to a set of fused hard spheres (the diameter of each protein atom is set at the distance where the Lennard-Jones potential energy equals the thermal energy k_BT): Now there are no serious overlaps of protein atoms. It has been verified that the structures before and after the minimization are almost indistinguishable in sight when they are drawn on a computer screen. It has been found that our energy function takes the lowest value for the native structure for all the seven proteins considered. The result is successful for both of the two minimization techniques employed. Thus, the native fold can be discriminated from the misfolded decoys with 100% accuracy. Moreover, the result is rather insensitive to the hard-sphere diameters of the protein atoms chosen and the value $7k_BT_0$: It is successful in the sense that the energy function becomes the lowest for the native structure, even when the diameters are simply set at the sigma values of the Lennard-Jones parameters or 90% of the sigma values, for example, and the value of the dehydration penalty is changed from $7k_BT_0$ to $6k_BT_0$ or $8k_BT_0$.

Here we define X and Y as

$$X=\xi/(k_BT_0)-\{\xi/(k_BT_0)\}_{\text{Native}}, \quad (14)$$
$$Y=-TS/(k_BT_0)-\{-TS/(k_BT_0)\}_{\text{Native}}, \quad (15)$$
$$X+Y=F-F_{\text{Native}}, \quad (16)$$

where the subscript "Native" denotes the value for the native structure. The plot of Y against X is shown in Figure 17 where the data for all the seven proteins considered are collected. X and Y share almost the same magnitude and these two factors are both important. On the whole, X and Y are anticorrelated for the following reason. When a protein takes a more compact structure, for example, the hydration entropy usually becomes lower. At the same time the burial of "CO" and "NH" occurs, but it is not always possible to completely make up for the break of hydrogen bonds with water molecules, giving rise to a larger value of ξ. There are significantly many structures giving Y<0. There are even more structures with X<0. However, there is no structure causing X+Y<0. The structures giving higher entropy of water than the native structure can certainly be constructed. However, such structures suffer serious total dehydration penalty. The structures undergoing only less total dehydration penalty than the native structure can also be constructed readily, but such structures give rise to seriously lower entropy of water. The native structure is optimized in terms of the sum of the two important factors (63). This holds true only for polypeptide chains with the amino-acid sequences selected by nature and for the folding in aqueous solution under physiological conditions. When the effect of the conformational entropy is added to F, it may be possible for us to deduce if a polypeptide chain with an artificial amino-acid sequence is foldable or to investigate the molecular mechanism of protein denaturation.

We consider the structural change of a protein in the isochoric process and concentrate on the total dehydration penalty ξ and the hydration entropy S. The calculation of ξ can be made with very high speed. The calculation of S, which is usually much more demanding, is also performed quite rapidly in the following prudent manner despite the use of a realistic molecular model for water. The simple protein model, a set of fused hard spheres, is acceptable when S is considered in the isochoric process. Since only the geometric feature of each protein structure is crucial, our morphometric approach becomes very powerful. In the approach no large computer memory is required and the calculation of F is finished in about 0.1 sec for one structure on the Itanium workstation. Another great advantage is that we can avoid the use of the protein force parameters which are more or less uncertain.

Our method thus developed is best suited to selecting the most stable structure from among the candidate structures. The number of the candidate structures is allowed to be huge, because in our method the energy function is calculated with minor computational effort. In the next stage, we intend to test our energy function for more databases of decoy structures (up to now, we have tested it for a total of fifteen proteins and always succeeded in selecting the native fold). Further, it may be possible to develop a practical tool for predicting the native structure of a protein from its amino-acid sequence, by combining our method with the bioinformatics techniques which can generate a variety of candidate structures. Our method is capable of handling much larger proteins than those considered above and can also be extended to analyses of the protein-protein interaction and protein aggregation. The application to the drug design is also

possible. In future studies, we intend to improve the method for calculating the total dehydration penalty.

4.7. Partial molar volume of a protein

There seem to be two misunderstandings about the partial molar volume (PMV) in the protein research community: The PMV is not clearly distinguished from the excluded volume (EV); and a less compact structure of a protein always has smaller PMV.

The PMV, which is denoted by V_M here, is the change of the system volume occurring upon the solute insertion in the isobaric process. Thermodynamically, the PMV is the pressure derivative of the solvation free energy expressed as

$$V_M=(\partial\mu/\partial P)_T. \quad (17)$$

The PMV is the key quantity in the argument of pressure denaturation of a protein (see Section 9.3).

Kirkwood and Buff (71) have derived the equation expressing the PMV in terms of the reduced solvent density profile near a spherical solute. Extending the equation to a polyatomic solute like a protein yields

$$V_M=\int\int\int \{1-g(x, y, z)\}\,dxdydz, \quad (18)$$

where $g(x, y, z)$ is the three-dimensional profile of the reduced solvent density. When the solvent is water and the solute is a protein, the ideal term is negligibly small and independent of the protein structure. Therefore, the ideal term is not included in Equation (18). The number of water molecules within the infinitesimal volume $dxdydz$ is $\rho_S g(x, y, z)dxdydz$ where ρ_S is the number density in bulk water. At distances which are sufficiently far from the protein surface, $g\rightarrow 1$. No overlap of an atom in the protein and a water molecule is allowed, and at positions where such an overlap occurs $g=0$. It is convenient to decompose the integration in Equation (18) into the integrations over the regions within which $g=0$ (region 1) and $g\neq 0$ (region 2), respectively. The integration over region 1 yields the EV generated by the protein. The EV is denoted by V here. The integration over region 2 is determined by the number density of water near the protein surface. The thickness of the surface-induced layer within which the number density of water differs from ρ_S is usually a few times of the molecular diameter of water. The integration over region 2 can be approximated by $-\zeta A$ where ζ is a parameter representing the average number density of water within the layer and A is the water-accessible surface area (ASA). It follows that the PMV is approximately given by (72, 73)

$$V_M=V-\zeta A. \quad (19)$$

ζ is dependent on the properties of the protein surface, temperature, and pressure. First, we consider a protein immersed in water at ambient temperature and pressure. A hydrophilic group in the protein makes a large, positive contribution to ζ because $g>>1$ on an average near it. By contrast, near a group which is hydrophobic enough to overcome the packing force, $g\sim 1$ or $g<1$ (see Appendix A) on an average, with the result that the group makes a small, negative contribution to ζ. Since hydrophilic and hydrophobic groups are almost irregularly distributed on the protein surface, the overall value of ζ becomes positive, and V_M is smaller than V. V and A vary greatly from structure to structure. If we compare two different structures, for example, it is rather frequent that one of them is larger in terms of V while the other is larger in terms of V_M.

How does the system volume change upon a structural transition of a protein? In general, when a protein is denatured, both of V and A becomes larger. Denoting the native structure and the denatured state by subscripts "1" and "2", respectively, we obtain

$$V_{M2}-V_{M1}=V_2-V_1-(\zeta_2A_2-\zeta_1A_1),\ V_2>V_1,\ A_2>A_1. \quad (20)$$

The PMV of the denatured state represents the average value of the PMV for an ensemble of denatured structures. Since a protein is characterized by the heterogeneity that hydrophilic and hydrophobic groups are rather irregularly distributed in the molecule, both of the total ASA for the hydrophilic groups and that for the hydrophobic groups increase upon the denaturation. On the whole, the increase for the hydrophobic groups should be larger. However, the surface properties on an average do not change greatly upon the denaturation, and we can employ the approximation $\zeta_2=\zeta_1=\zeta(>0)$. Equation (20) can then be rewritten as

$$V_{M2}-V_{M1}=V_2-V_1-\zeta(A_2-A_1),\ V_2>V_1,\ A_2>A_1. \quad (21)$$

The sign of "$V_{M2}-V_{M1}$" is determined by the complicated interplay of ζ□"V_2-V_1", and "A_2-A_1".

In the experiments, a protein is usually denatured by the addition of acid, and the PMV difference between the native structure and the denatured state is determined by measuring the system-volume change upon the denaturation. The protein surface in the presence of acid (under low-pH conditions) has many groups with large, positive charges. The net charge takes a large, positive value and the surface is highly hydrophilic. Due to the high hydrophilicity (or the electrostatic repulsions between positively charged groups) a set of rather extended structures with large ASA are stabilized. ζ takes a very large, positive value. "$-\zeta(A_2-A_1)<<0$" predominates over "$V_2-V_1>0$" with the result that the PMV is much smaller for the acid-denatured state than for the native structure: The system volume decreases to a great extent upon the denaturation. (In a strict sense, the solvent conditions before and after the acid addition are different. For this reason, Equation (20) with $\zeta_2>>\zeta_1$ may be more appropriate. "$-(\zeta_2A_2-\zeta_1A_1)<<0$" predominates over "$V_2-V_1>0$" with the result that the PMV is much smaller for the acid-denatured state, leading to the same conclusion.)

It is quite dangerous to generalize the above experimental result and conclude that a less compact (a

more extended) structure always has smaller PMV. The result is not applicable to the heat- and pressure-denatured states (the denaturation in the absence of acid). Take the pressure-denatured state, for example. The PMV is smaller for the state than for the native structure. However, it is erroneous to consider that the structures in the state are rather extended like those in the acid-denatured state. (The pressure-denatured state is discussed in detail in Section 4.8.) When a protein folds in aqueous solution under physiological conditions, unless the burial of hydrophilic groups predominates over that of hydrophobic groups, the system volume should decrease. This seems to be valid from the argument described in Section 4.5 as well. As stated in Section 4.8, however, the PMV of the native structure is never the smallest. A protein is denatured by applying an extremely high pressure, but the structures in the denatured state are far from the random coils.

We emphasize that the PMV is remarkably influenced by the solvent environment. As a striking example, the PMV of a small solute molecule is positive in water at ambient temperature and pressure, whereas in water with medium densities in the supercritical state it takes an abnormally large, negative value. (This is ascribed to the formation of a layer around the solute within which the water density is much higher than in the bulk (74).)

Some researchers claim that the EV of the native structure is larger than that of an extended structure due to the small void spaces in the interior of the former, but this claim is wrong. In the lower picture in Figure 10, for example, even when the three side chains are not closely packed and make a small space which water molecules cannot enter, there is certainly an overlap of the excluded volumes (the space shadowed has a finite volume). The total excluded volume in the lower picture is smaller than that in the upper picture. We have compared the EV-values of the native structure and a number of random coils using an elaborate calculation method (75) (of course, the void spaces in the interior of the native structure are taken into consideration) and verified that the EV of the native structure is always much smaller. The EV of a fully extended structure is even much larger than that of a random coil.

Last, we comment on how to calculate the PMV of a protein. As mentioned above, a dense layer is formed near a hydrophilic group while a depleted layer is formed near a hydrophobic group. The 3D-RISM theory (54, 55) is capable of accounting for the polyatomic structure of a protein. For water molecules, however, it suffers the problems caused by the site-site treatment described in Section 3.8. Our calculation results have shown that the 3D-RISM theory gives a remarkably dense layer even near a hydrophobic group (56). It follows that the whole surface of the protein becomes unrealistically hydrophilic, causing too large a value of ζ. This shortcoming does not become serious for the absolute value of the PMV of a protein structure because the PMV is not far from the EV. For a difference between two structures in the PMV, however, the 3D-RISM theory becomes problematic: There is a tendency that the PMV of a more extended structure is relatively smaller. It seems that this inappropriate prediction of the 3D-RISM theory has enhanced the misunderstanding in regard to the PMV arising from the experimental studies on the acid-induced denaturation. When the protein is modeled as a fused hard spheres and water is taken to be hard spheres, the water density near a hydrophilic group is underestimated while that near a hydrophobic group is overestimated, leading to a fortuitous cancellation of errors (72, 73) and a better result (56).

4.8. Molecular mechanism of pressure denaturation of a protein: physical similarity to crystal nucleation known for a single-component system of hard spheres

A protein folds into a unique native structure and becomes functional in aqueous solution under physiological conditions. However, the native structure is unfolded by various perturbations such as the addition of chemical substances, the change in the temperature or pH, and the application of a high pressure. Investigating those processes will provide physical insights into the folding/unfolding transition of proteins. Above all, the pressure-induced unfolding is one of the most interesting subjects. Recent experimental studies have indicated that the ensemble of unfolding pathways for pressure denaturation is inherently different from those for heat or chemical denaturation (76, 77). This implies that a specific viewpoint is necessary for uncovering the mechanism of pressure denaturation. One might think that the native structure with a very small excluded volume, in which the backbone and side chains are closely packed with little space in the interior (40), is further stabilized through the entropic effect by applying a higher pressure. However, the behavior of the entropic effect is not that simple.

Let us consider a pressure-denatured state and the native state of a protein immersed in aqueous solution. The pressure-denatured state and the native state, respectively, represent an ensemble of unfolded structures stabilized at high pressures and that of uniquely folded structures stabilized at low pressures. The free energy of the protein-aqueous solution system is lower for the native state at low pressures while it is lower for the denatured state at high pressures. The difference between the two states in the conformational entropy is independent of the pressure or smaller at high pressures due to the constraint caused by denser water, and the conformational-entropy effect cannot be a driving force in pressure denaturation. Hereafter, we consider several representative structures in the denatured state and refer to them simply as "denatured structures". Within the framework of classical mechanics, the intramolecular energy for any structure remains unchanged against a pressure change. It follows that the change in the hydration free energy is the key to pressure denaturation. For the denaturation to occur, "μ of a denatured structure minus μ of the native structure", which is positive at low pressures, must decrease to a significant extent as the pressure P increases and eventually become negative. Therefore, the partial molar volume (PMV) (see Equation (14)) of the denatured structure is to be smaller than that of the native structure.

The hydration free energy consists of the

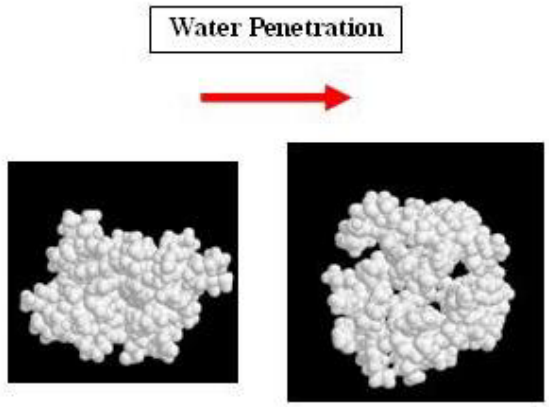

Figure 18. A swelling structure featuring pressure-induced denaturation (left) and the native structure (right) of protein G.

energetic and entropic components. According to the experimental results (76-82), nonpolar side chains are more separated in a denatured structure with water molecules penetrating its hydrophobic core. When the penetration occurs, the break of hydrogen bonds of water is unavoidable, leading to a loss in terms of the hydration energy. There must be an even larger gain in terms of the hydration entropy, an increase in the water entropy in the system. We have made a statistical-thermodynamic analysis (72, 73) focused on the effect of the translational motion of water molecules by employing the three-dimensional integral equation theory (6, 42) combined with hard-body models ($\mu=-TS$ where S is the hydration entropy). Some of the important results are summarized below.

1. The excluded volume (EV) and water-accessible surface area (ASA) are two essential parameters for a protein structure. A structure possessing smaller PMV than the native structure features moderate compactness, correspondingly small EV, but very large ASA, which can readily be understood from Equation (19). Such a structure is characterized by the cleft and/or swelling and water penetration into the interior. This result is in good accord with the experimental observations (76-82).

2. At low pressures the water entropy is almost maximized when a protein takes the native structure, whereas at high pressures the water entropy becomes higher when the transition to the structure mentioned in (1) occurs. (In the isobaric process, the system volume slightly decreases and part of the entropic gain upon the transition considered in the isochoric process is converted to a corresponding enthalpic gain, but *the free-energy gain is the same*. See Section 3.5.)

3. As described in (1), a structure, which is only moderately less compact than the native structure but has much larger ASA, turns more stable than the native one at an elevated pressure. In another solvent whose molecular size is 1.5 times larger than that of water, however, the inversion of the stability does not occur any longer. It has been inferred from experimental results (83) that water is crucial for pressure denaturation. Our theoretical analysis has supported this inference with the physical interpretation that the exceptionally small molecular size of water is responsible for the crucial importance of water in pressure denaturation.

4. A random coil features very large ASA but too large EV with the result that it has larger PMV than the native structure. It becomes relatively more destabilized with rising pressure, irrespective of the molecular size of the solvent.

5. A fully extended structure, which is unrealistic, has even larger PMV than the random-coil state.

6. The inequality for the PMV, "pressure-denatured structure < native structure < random coil < fully extended structure", holds at both low and high pressures.

The entropically induced denaturation can be interpreted as follows. The presence of a water molecule generates an excluded volume for the other water molecules. This *water crowding* becomes serious when the pressure is highly increased. For water as well as for the hard-sphere solvent, in the morphometric form of Equation (9) applied to $-S/k_B$ at high pressures, $C_1>0$, $C_2<0$, and their absolute values are very large. Structures not only with large ASA but also with small EV are stabilized. Due to the serious crowing, the so-called packing force becomes remarkably strong. Structures with much larger ASA but with sufficiently small EV, which is characterized by the penetration of water molecules into the interior and the contact of many water molecules on the surface, is more favored. This relaxes the restriction for the translational motion of the water molecules *which are well outside the protein* while that of the water molecules in the interior and on the surface is largely restricted. The former effect arises at a sufficiently high pressure: The total entropy of water becomes all the higher when the protein is denatured in the manner described above. The entropic effect discussed so far is a major cause of the solute hydrophobicity. At a higher pressure the hydrophobicity is strengthened in the sense that the water crowding is serious and the hydration free energy becomes higher. The previously suggested concept (82, 84), the weakening of the hydrophobic interaction between nonpolar side chains is responsible for pressure denaturation, is inconsistent with our view.

The structure of protein G shown on the left side of Figure 18, which has smaller PMV than the native structure shown on the right side, has the swelling and well captures the characteristics of pressure-denatured structures. The penetration of water molecules into the protein interior can be verified by investigating the reduced solvent-density profile $g(x, y, z)$. Figure 19 shows $g(x, y, z)$ along an example line for the structure featuring the swelling. At the separations which are sufficiently far from the protein surface, g is unity. Near the surface, g is oscillatory and takes a rather large value at contact. In the region where no solvent molecule can be present, g is zero. The penetration of water molecules into a narrow, confined space in the interior is characterized by very sharp peaks of g. The figure certainly indicates this type of penetration.

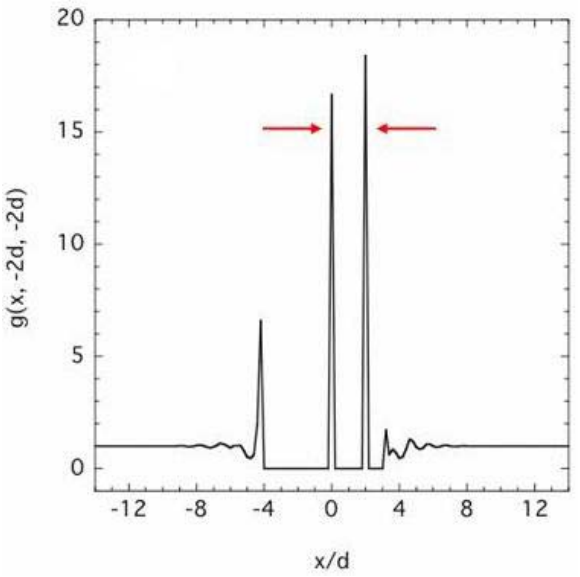

Figure 19. Reduced density profile of water indicating water penetration into the protein interior. Here, d denotes the diameter of water molecules (d=d_S). The very sharp peaks of the profile are indicated by the red arrows.

Very recently, we have made a further analysis (52) using the angle-dependent integral equation theory (24-32) combined with the morphometric approach (50) in which the multipolar model (25, 26) is adopted for water. The hydration entropy of a protein with a fixed structure is decomposed into

i. the component arising only from the excluded volume which is calculated using the Asakura-Oosawa theory (1, 2),

ii. the protein-water pair correlation component (24, 32, 52) (hydration entropy at the pair correlation level) other than component (i),
and

iii. the protein-water-water triplet and higher-order correlation components (24, 32, 52) (hydration entropy at the triplet and higher-order correlation levels).

Only the water molecules near the protein contribute to component (ii), while all the water molecules in the system contribute to components (i) and (iii). Component (iii) also contains the information on the water structure near the protein. The translational and rotational motions of water molecules are restricted upon the protein insertion. Components (ii) and (iii) are further decomposed into contributions from the translational and rotational restrictions. The pair correlation component represents how the motion of each of water molecules is restricted upon the protein insertion. The motion of a water molecule is influenced by the motions of the other water molecules, and component (iii) represents how the details of the influence are changed upon the protein insertion. The hydration entropy and its components are strongly dependent on the protein structure. First, it has been verified that the swelling structure considered in our earlier work (72, 73), which has only moderately less compact than the native structure but has a much larger ASA, turns more stable than the native structure at an elevated pressure. The most important finding is that at high pressures the denaturation accompanies a loss of the translational and rotational entropies at the pair correlation level and a much larger gain of the translational entropy at the triplet and higher-order correlation levels. This implies the following: The translational and rotational motions of water molecules penetrating the protein interior and contacting the protein surface are largely restricted; but the penetration and the contact lead to a great reduction of the translational restriction *for the water molecules that are sufficiently far from the protein*. The entropy of the whole water in the system increases upon pressure denaturation. If we consider component (i) only, the conclusion is that the native structure is increasingly more stabilized as the pressure becomes higher. The conventional concept, which looks only at the water structure in the vicinity of the protein, is not capable of elucidating the molecular mechanism of pressure denaturation. (Appendix C gives some information on the first coefficient in the morphometric form of the components considered for the hydration entropy.)

As described in Section 4.3, at high pressures water takes on the characteristics of hard spheres. In Equation (9) applied to the hydration free energy, C_2 is positive at low pressures but turns negative at high pressures. From this standpoint, a structure with smaller ASA is more favored at low pressures while that with larger ASA is more favored at high pressures. On the other hand, a structure with smaller EV is always favored irrespective of the pressure. These are quite consistent with the result described above, "at high pressures structures like the swelling structure are stabilized". It is interesting to note that when the multipolar model (not the hard-sphere model) is employed for water, the inequality for the PMV at high pressures is "pressure-denatured structure < native structure < random coil < fully extended structure" that is the same as the inequality in the hard-sphere model. At low pressures, however, it is "native structure < pressure-denatured structure < random coil < fully extended structure" (this does not alter our conclusions on the molecular mechanism of pressure denaturation).

By the way, in a single-component system of hard spheres, part of the hard spheres forms crystal nuclei when the packing fraction becomes quite high. This phenomenon related to the Alder transition (85-87) is counterintuitive because the fluid phase should be entropically more stable than the crystal phase. The crystal nucleation could be interpreted as follows: The translational motion of the hard spheres in the crystal nuclei (and that of the hard spheres which are in contact with the crystal nuclei) is largely restricted while the translational restriction for the other hard spheres is greatly reduced, leading to an overall entropic gain. Pressure denaturation of proteins is physically similar to the crystal nucleation in the following two respects: (1) The denaturation and the nucleation are both entropically driven; and (2) if the attention is paid only to the water molecules penetrating into the protein interior

or to the hard spheres forming the crystal nuclei, the entropy appears to decrease and the basic physics can never be understood. (If the packing fraction exceeds a threshold value, due to the extreme crowding, the fluid phase in which each hard sphere tries to move arbitrarily becomes less stable than the crystal phase. The system entropy is higher when the hard spheres are regularly arranged and each hard sphere moves within its surrounding space. As a result, the whole system is crystallized, leading to the Alder transition.)

4.9. Heat and cold denaturations of a protein

We briefly refer to heat and cold denaturations (88, 89) of a protein. It has been verified by experiments (90) that the loss of the conformational entropy (CE) upon protein folding increases to a great extent as the temperature becomes higher. The CE is closely related to the torsion energy of a protein molecule. The dihedral angle giving high torsion energy is not allowed at a low temperature. As the temperature increases, the allowed range of the dihedral angle becomes increasingly wider, leading to larger CE of an unfolded conformation. The CE of the native structure does not become significantly larger due to its conformational constraints. It follows that the CE loss upon the folding becomes larger with increasing temperature. The CE loss multiplied by the absolute temperature further increases as the temperature becomes higher, and this effect should be a major cause of heat denaturation.

It has recently been found that yeast frataxin (89) exhibits cold denaturation above 273 K in the absence of chemical denaturants and cryosolvents. It is interesting that the cold-denatured structures are completely unfolded like the heat-denatured structures. Cold denaturation is characterized by a significantly large entropic loss and en even larger enthalpic gain. The change in the specific heat is positive. We are now pursuing the molecular mechanism of cold denaturation using the angle-dependent integral equation theory (24-32) combined with the morphometric approach (50). The preliminary results (91) are summarized below.

The temperature dependence of the hydrophobicity of nonpolar groups provides an important clue to the molecular mechanism. We have analyzed the components of the thermodynamic quantities of hydration which are determined by the excluded volume (EV) and by the water-accessible surface area (ASA) and the surface curvature (SC), respectively. When the temperature is lowered, the ordered structure with enhanced hydrogen bonds of water molecules is formed near nonpolar groups. The enhancement is not strong but becomes significant for unfolded structures with large ASA. At lower temperatures, those structures are relatively more destabilized in terms of the ASA- and SC-dependent component of the hydration entropy but stabilized in terms of the ASA- and SC-dependent component of the hydration energy. The temperature dependence of the changes of water entropy and energy upon the denaturation are governed by the ASA- and SC-dependent components. The change in the specific heat upon cold denaturation is also governed by these components. At low temperatures, the hydrogen bonding of water near nonpolar groups is enhanced. For unfolded structures, larger part of the heat added is consumed for the break of the hydrogen bonds, giving rise to a positive change in the specific heat.

As for the free-energy change of water upon the denaturation, which is more important, it exhibits different behavior. At lower temperatures, both the native structure and unfolded structures are *less hydrophobic* in the sense that $\mu/(k_BT)$ (μ is the hydration free energy) is significantly reduced (it should be noted that μ is even more reduced). However, the reduction is greater for a structure with larger EV. This feature is ascribed to the effect of the EV-dependent component of the hydration entropy (the EV-dependent component of the hydration energy has the opposite effect that is considerably smaller): The translational-entropy effect arising from the water in the whole system, by which the native structure is stabilized relative to the unfolded structures, is considerably less powerful when the temperature is lowered, leading to cold denaturation. As mentioned above, due to the structuring of water near the protein surface at lower temperatures, unfolded structures with large ASA are relatively more destabilized in terms of the water entropy but stabilized in terms of the water energy. In terms of the free energy, however, the destabilization and the stabilization are almost cancelled out.

It is also shown that polar and charged groups become more hydrophilic as well as nonpolar groups become less hydrophobic, which should make a significant contribution to cold denaturation.

5. MOLECULAR RECOGNITION BETWEEN GUEST LIGANDS AND HOST ENZYMES

5.1. Statistical-mechanical analysis focused on the effect of translational motion of water molecules

A host enzyme binds a particular guest ligand with extremely high selectivity, which is often referred to as the lock-key interaction. Elucidating the mechanism of this "molecular recognition" is of great interest not only from the scientific viewpoint but also for various applications such as designs of drugs and bio-sensors.

We have performed an analysis on the lock-key interaction (6, 7, 92) using the three-dimensional integral equation theory (6, 42) combined with a hard-body model. The analysis is focused on the effect of the translational motion of water molecules. Solute 1 and solute 2 illustrated in Figure 20 are considered. Solute 1 is a big hard cube with a hemispherical cavity with diameter $d_1=5d_S$ and the length of a step edge is $L=10d_S$. Solute 2 is a big hard sphere with diameter d_2. The two solutes are immersed in small hard spheres with diameter d_S forming the solvent. We test several different diameters of the big sphere that are smaller than ($d_2=3d_S$ and $4d_S$), equal to ($d_2=5d_S$), and larger than ($d_2=6d_S$) the diameter of the cavity, respectively. A great advantage of the three-dimensional integral equation theory is that the spatial distribution of the potential of mean force $\Phi_{12}(x, y, z)$ is obtained only in a

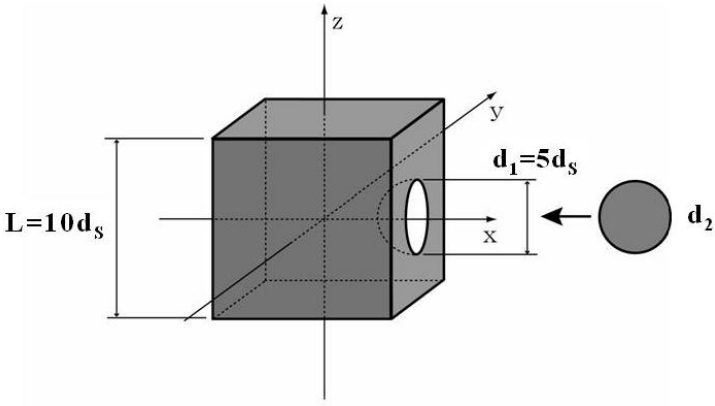

Figure 20. Models of "lock" and "key". A big hard cube with a hemispherical cavity (lock) with diameter $d_1=5d_S$ and a big hard sphere (key) with diameter d_2. The length of a step edge of the cube is $L=10d_S$. The two big bodies are immersed in small hard spheres with diameter d_S forming the solvent (the small spheres are not shown here).

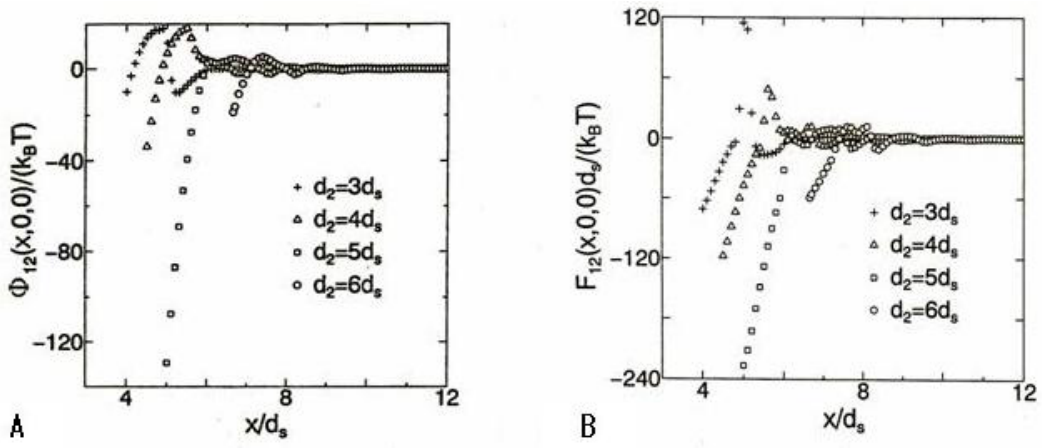

Figure 21. (a) Lock-key interaction represented by entropic interaction between the two big bodies along the x-axis $\Phi_{12}(x, 0, 0)$. T, k_B, and d_S denote the absolute temperature, Boltzmann constant, and diameter of the small spheres, respectively. Four different values are tested for the diameter of the big sphere d_2. (b) Lock-key force defined by $F_{12}(x, 0, 0)=-\partial\Phi_{12}(x, 0, 0)/\partial x$.

single calculation. This advantage is not shared by the computer simulation. By analyzing $\Phi_{12}(x, 0, 0)$, we can obtain information on the lock-key interaction. The hemispherical cavity and the big sphere correspond to the lock (active site of a host enzyme) and the key (guest ligand), respectively.

The potential of mean force $\Phi_{12}(x, 0, 0)$ calculated is shown in Figure 21(a). Stabilization occurs when the key is at contact with the lock: The stabilization free energy (the free-energy gain of the solvent) for the key that exactly fits in the lock ($d_2=5d_S$) is far larger than for the other keys. For $d_2=5d_S$, the volume of the excluded-region overlap occurring when the big sphere touches the cavity surface is estimated to be ~5.7 times larger than that in the case where the big sphere touches a flat surface. Nevertheless, the stabilization free energy in the former is ~20 times larger than in the latter, which implies a complete failure of the Asakura-Oosawa theory (1,2) (the physical origin of this failure is described in earlier publications (6, 7)). An even more important result is that there are high free-energy barriers for the keys smaller than the lock to overcome before getting in contact with the lock. The mean force $F_{12}(x, 0, 0)=-\partial\Phi_{12}(x, 0, 0)/\partial x$ is shown in Figure 21(b). The force curve between one of the smaller keys with $d_2=3d_S$ and $4d_S$ and the lock has a strongly repulsive peak at surface separations almost equal to and slightly larger than d_S, leading to the high free-energy barrier. As the key size reduces, the repulsive force becomes stronger. At surface separations almost equal to and slightly larger than d_S, small spheres, which are densely packed within the domain confined between the two surfaces, remain. The thermal pressure due to the remaining small spheres acts as a repulsive component of the induced force. The remaining small spheres must be removed before the key touches the lock surface. In reality, they are removed by the interplay of the conformational fluctuation of the lock and the three-

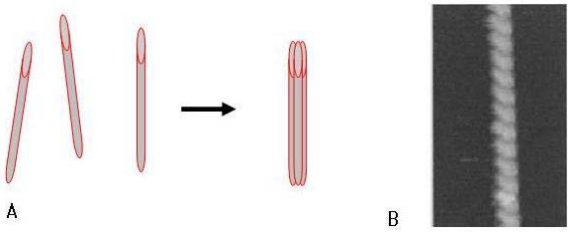

Figure 22. (a) Lateral contacts of long cylindrical units. (b) Double-helical structure formed by the twisting of two cylindrical units, which is observed in real experiments.

dimensional motion of the key. These dynamic aspects are not taken into account in the present analysis. However, when the key is too small, the removal becomes very difficult to achieve because the key is strongly repelled by the remaining small spheres.

It is remarkable that very high size and shape selectivity in the lock-key interaction arises from the purely entropic effect due to the translational motion of water molecules.

One might think that the real water molecules (not hard spheres) do not enter the channel between the lock and key surfaces. This is true if the surfaces are both highly hydrophobic. In usual cases, however, the surfaces consist of hydrophobic and hydrophilic groups. As a result, the behavior of water molecules is more like that of hard spheres. The concept, "when two extended hydrophobic surfaces approach each other, the water confined between the surfaces eventually vaporizes", is not applicable to this case.

5.2. Relevance to experimental observations

There is a large amount of experimental data on changes in thermodynamic quantities upon the binding of a receptor and a ligand. Despite the large loss of the conformational entropies of the receptor and the ligand, there are many examples showing that the enthalpy and entropy changes are both positive even at room temperature (93, 94). This manifests that the entropic effect originating from the translational motion of the water molecules which are present in the system is a major driving force in the binding process.

6. FORMATION OF ORDERED STRUCTURE BY AGGREGATION OF PROTEIN MOLECULES

6.1. Regularity and symmetry of aggregates

Aggregates (quarterly structures) of protein molecules as well as single protein molecules play essential roles in biological systems. These aggregates feature "regularity" and "symmetry". We believe that the translational motion of water molecules is a principal driving force in the formation of the aggregates. For example, DNA and a microfilament of actin possess the double-helical structure. The formation of the double-helical structure leads to a great reduction of the excluded volume for water molecules. It is generally believed that the double-helical structure of DNA is formed by the intramolecular hydrogen bonds between bases. However, the intramolecular hydrogen bonding in aqueous solution accompanies the serious dehydration penalty and can give rise to an overall energy loss.

6.2. Molecular mechanism of amyloid-fibril formation

When misfolding or denaturation of a protein occurs for some reason, the misfolded or denatured proteins often form fibril-like aggregates called "amyloid fibrils". Though the amyloid-fibril formation is a typical example having pathological influences on life, its molecular mechanism should be the same as that of the formation of functional, indispensable aggregates of proteins. The entropic effect arising from the translational motion of water molecules plays crucial roles in the formation of these aggregates.

The characteristics of the amyloid-fibril formation (95-105) which are common to many of the experimental observations are as follows: (i) the aggregation does not occur unless the proteins are denatured; (ii) it takes a rather long time for sufficiently large aggregates acting as nuclei to be formed, but the succeeding growth of the nuclei is rapid; (iii) though the structures of the fibrils can be variable, the most common and fundamental feature is the stacking of extended, thin beta-sheets; and (iv) when a foreign fibril-like matter is introduced, it acts as a nucleus. According to an experimental result, a number of β-strands form extended, thin beta-sheets through intramolecular hydrogen bonds, the beta-sheets stack together to form a larger-scale unit, and the units stack together regularly on a wall surface (95). It has been reported that extended, thin cross beta-sheets form a cylindrical unit by stacking together (96), and the units contact one another laterally as illustrated in Figure 22(a) or twist together to form a double-helical structure as shown in Figure 22(b) (97).

We have carried out a statistical-mechanical analysis (106-108) focused on the effect of the translational motion of water molecules and obtained the following results:

(1) Nearly spherical proteins with the native structure are stable as separate molecules due to high free-energy barriers in the entropic interactions between protein molecules. However, proteins with high asphericity in their overall shapes can readily aggregate.
(2) When proteins aggregate, the assurance of protein-protein hydrogen bonding is crucially important to compensate the dehydration penalty. There can be two typical types of protein aggregation which allows as many protein-protein hydrogen bonds as possible: lateral contacts of α-helices with long cylindrical shapes and stacking of extended, thin beta-sheets. The latter is more stable because the restriction for the translational motion of water molecules is reduced to a greater extent.
(3) As an important matter, the most stable structure of an isolated protein (i.e., the native structure) is totally different from the structure of a protein in the most stable aggregate.

The result of (1) can readily be understood from the argument described in Section 3.6 and Figure 8. It is

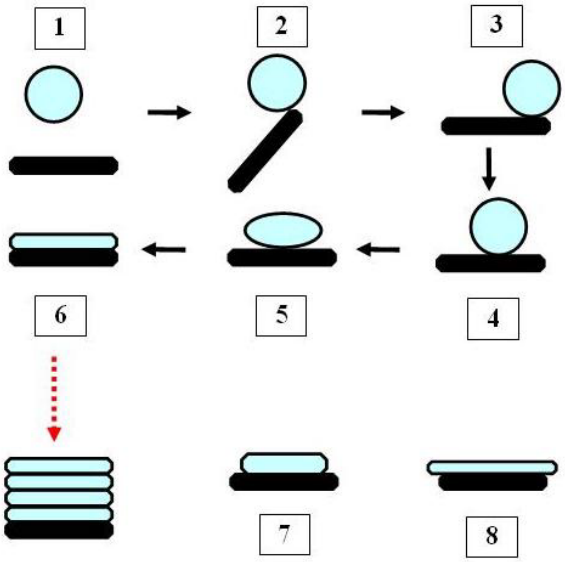

Figure 23. What will happen if a big rigid disc (its shape is not changeable) is introduced to big soft spheres (their shapes are changeable) immersed in small spheres? Even the introduction of the single big rigid disc is capable of changing a number of big soft spheres into discs with the same shape, and a cylindrical aggregate can continue to elongate with the diameter unchanged.

consistent with the experimental evidence (i) that the denaturation of proteins (i.e., the collapse of a nearly spherical shape) is the initiator of the amyloid-fibril formation. It is also closely related to the fact that a protein molecule needs to be isolated from the other molecules through the protection by shaperonin until the molecule accomplishes the folding to its native structure with a nearly spherical shape. The result of (2) does not contradict the experimental evidence (iii). Even after proteins are denatured, it will take a long time for them to reach the stage of the beta-sheet stacking. This is because an aggregate which is not large enough is broken due to the effect of the conformational and translational entropies of protein molecules. Once a sufficiently large aggregate, which is stabilized by the entropic excluded-volume effect, is formed, it will work as a nucleus. The experimental evidence (ii) can thus be understood. It appears that the patterns illustrated in Figure 22 can be explained only by the entropic effect. When this effect is dominant, once a fundamental unit which is stable enough is introduced to the system, its growth pattern is determined by the geometric feature of the unit. This is relevant to the experimental evidence (iv).

6.3. Flexibility and adaptability of protein structure

Suppose a big rigid disc is introduced to big soft spheres immersed in small spheres as shown in Figure 23. The shapes of the soft spheres can be changed while the shape of the rigid disc cannot. When a big sphere is isolated, the spherical shape persists because it generates the least excluded volume for the small spheres. However, the big sphere can touch the edge of a big disc because there is no high free-energy barrier for this type of touching. When this occurs, the big sphere moves into the flat surface of the disc, changing the shape into the same disc (see configuration 6 in Figure 23). Here, the free energy of the small spheres in configuration I (I=1, ..., 8) is denoted by F_I and the difference, F_J–F_I , is expressed by ΔF_{IJ} . It can be shown within the framework of the Asakura-Oosawa theory (1, 2) that ΔF_{46} is approximated by (106)

$$\Delta F_{46}=-(3-2/a)\eta_S(d_L/d_S)^2 k_B T, \quad (22a)$$
$$a=d_D/d_L, \quad (22b)$$
$$a>1, \quad (22c)$$

where d_L is the diameter of a big sphere ($d_L>>d_S$), the upper and lower surfaces of a big rigid disc is assumed to be circles, and d_D is the diameter of the circles ($d_D>>d_S$). The volumes of the big sphere and the big rigid disc are assumed to be equal. In configuration 7 or configuration 8 the big sphere has changed into a big disc with diameter xd_D whose volume is equal to that of the rigid disc. ΔF_{76} and ΔF_{86} are approximately given by the following (106):

$$\Delta F_{76}=-12\eta_S(d_D/d_S)(l_D/d_S)\{(1-x)/x\}k_B T, \quad (23a)$$
$$x<1, \quad (23b)$$

$$\Delta F_{86}=-3\eta_S[(d_D/d_S)^2(x^2-1)/2-4(d_D/d_S)(l_D/d_S)\{(x-1)/x\}]k_B T, \quad (24a)$$
$$x>1. \quad (24b)$$

Here, l_D is the height of the big rigid disc. From these equations one sees that for large d_D/d_S the free energy of the small spheres in configuration 7 or in configuration 8 is much higher than that in configuration 6: configurations 7 and 8 are not likely to occur. ΔF_{14} is approximated by (106)

$$\Delta F_{14}=-3\eta_S(d_L/d_S)k_B T. \quad (25)$$

The free-energy change ΔF_{16} is governed by ΔF_{46} because $|\Delta F_{46}|>>|\Delta F_{14}|$ for large d_L/d_S.

The whole process illustrated in Figure 23 is driven to attain almost the largest decrease in the excluded volume for the small spheres and occurs sequentially. If N spheres are changed into discs to be incorporated in the cylindrical aggregate formed, the free-energy change reaches $\sim N\Delta F_{46}$ that can be surprisingly large: In the case of d_L/d_S=5, a=2, and N=10, for example, $N\Delta F_{46}$ reaches $-190k_B T$ when the small spheres are water molecules. Thus, even the presence of a single big rigid disc is capable of changing a number of big spheres into discs with the same shape, and the cylindrical aggregate continues to elongate with the diameter unchanged.

The interesting behavior illustrated in Figure 23, which arises from the effect of the translational motion of water molecules, might be related to the fact that even a single prion with a pathological structure successively changes prions with the native structure to those with the same pathological structure. This is an example having ill influences on life. To change the subject to the aggregate which is indispensable to life, the protein structure

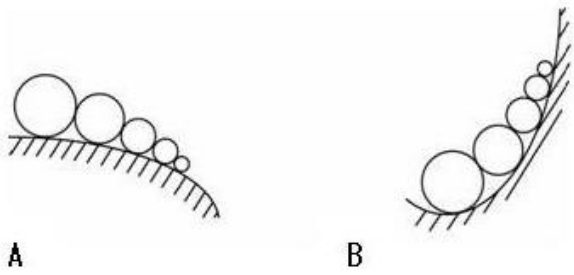

Figure 24. (a) Ordered structure formed by a convex surface and big particles with different sizes. (b) Ordered structure formed by a concave surface and big particles with different sizes.

possesses the flexibility and adaptability in the sense that a protein molecule can be integrated into a functional system by changing its own molecular structure in a suitable way. This can also be relevant to the behavior described in the last paragraph.

Though water plays critical roles in sustaining life, they can possibly cause serious problems such as the amyloid-fibril formation. Presumably, water also plays central roles in giving rise to aging and disease, which clearly conflicts with the title of this review article.

6.4. Relevance to experimental observations

In usual experiments for the amyloid-fibril formation, the proteins are first unfolded by the addition of acid. The acid-unfolded proteins do not aggregate, however, due to the electrostatic repulsion between groups with positive charges. When salts are added, the charges are screened by counter ions with negative charges, with the result that the entropic interaction effectively drives the proteins to aggregate. According to the experimental results reported by Goto *et al.* (108), when the salt concentration is sufficiently low, nuclei added to the system grows to form the amyloid fibrils. When the salt concentration is too high, the proteins form irregular aggregates. This is because, as shown by us (109), an attractive force acts between groups with charges in the same sign due to the salt effect. Thus, when a force other than the entropic force dominates, irregular aggregation occurs but "regularity" or "ordering" is not exhibited.

Goto *et al.* (110) has reported the changes in thermodynamic quantities upon the amyloif-fibril formation. Below 286 K the enthalpy and entropy changes are both positive, which indicates that the fibril formation is entropically driven. It is remarkable that the entropy change is positive despite the large loss of the conformational and translational entropies of protein molecules. The large loss is overcome by an even larger entropy gain of the water that is present in the system.

Very recently, it has been reported that the amyloid-fibril formation accompanies a large increase in the system volume (111). We can deduce the following: (1) In the fibril formation the contact of hydrophilic groups is dominant as compared to that of hydrophobic groups and that of hydrophilic and hydrophobic groups; and (2) as argued in Section 3.5 the protein-protein intermolecular energy gain should be quite large though the entropic excluded-volume effect is still essential. In the experiment, however, the amyloid-fibril formation occurs under a low-pH condition after the addition of acid and salts. As discussed in Section 4.7 in detail, it is possible that this type of experiment does not simulate the fibril formation in aqueous solution *under physiological conditions*.

We believe that the fibril formation leads to a system-volume decrease in aqueous solution under physiological conditions as long as the contact of hydrophobic groups dominates. At very high pressures, however, *the dissolution of the fibrils results in a system-volume decrease*. This is because water takes on characteristics of hard spheres (see Sections 4.3 and 4.8) and high density layers of water molecules are formed near both hydrophilic and hydrophobic groups: A state with a much larger water accessible surface area (ASA) has a smaller volume. From the standpoint of the free energy, a state with smaller ASA is more favored at low pressures while a state with larger ASA is more favored at very high pressures.

In any case, the process of the fibril formation is remarkably affected by the solvent specifications such as the pressure, temperature, and pH. It is quite dangerous to generalize the experimental results obtained under a particular solvent condition. The effects of the solvent specifications are complicated and to be investigated further. We emphasize that regardless of the decrease or increase in the system volume, the excluded volume for water molecules always decrease upon the fibril formation.

7. OTHER ORDERING PROCESSES IN BIOLOGICAL SYSTEMS

7.1. Specificity in associations between lipids and proteins

The free-energy gain of the small spheres occurring when a big sphere contacts a surface is remarkably dependent on the surface curvature if η_S is sufficiently high and d_L/d_S is large enough. It can be shown that the free-energy gain follows the order, "a concave surface with larger curvature > a concave surface with smaller curvature > a flat surface > a convex surface with smaller curvature > a convex surface with larger curvature" (7). Moreover, the differences are magnified as d_L becomes larger.

The above result suggests the following. Suppose a surface with changing curvature and big spheres with a size distribution are immersed in small spheres. If the surface is convex, a bigger sphere preferentially contacts the surface portion with a smaller curvature. The biggest sphere contacts the surface portion with the smallest curvature, and there is almost no chance for a smaller big sphere to contact that portion. The second biggest sphere then contacts the portion with the second smallest curvature. Thus, the ordered structure depicted in Figure 24(a) is entropically formed. A similar discussion can be made for a concave surface for which a bigger sphere preferentially

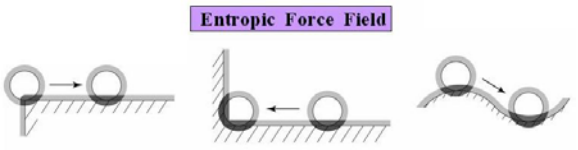

Figure 25. Control of movement of big particles by entropic force field generated by passive microstructure of wall surface. The big particles tend to be moved in a specific direction so that the overlap of the excluded volumes shadowed can be increased.

contacts the surface portion with a larger curvature, and a probable ordered structure is shown in Figure 24(b). In (a) or (b) of the figure, the free energy of the small particles increases significantly if any two of the big spheres are exchanged. Thus, in contacts of big spheres with surfaces, great specificity between the surface curvature and the big-sphere size is provided (7).

In biological systems, the surface and big spheres correspond to a membrane and proteins (a different protein species has a different size), respectively, immersed in water molecules acting as small spheres. The membrane contains multiple species of lipids and the regions with different curvatures have different local compositions of lipids. The great specificity between the surface curvature and the big-sphere size, which arises from the entropic excluded-volume effect, may lead to the specificity in associations between lipids and proteins. (In the case of a hard wall, a big particle only contacts the wall surface. If the wall is soft like the membrane, the big particle is driven to be buried within the membrane by the excluded-volume effect.)

7.2. Can the motion of biomolecules be controlled?

The illustration shown in Figure 25 indicates that the big-particle motion can be controlled using passive surface microstructures creating localized entropic force fields that repel or trap the particles and induce their drift in a predetermined direction (7, 16). The big particles tend to be moved in a specific direction so that the overlap of the excluded volumes shadowed can be increased. For example, a big particle can be repelled from a step edge, trapped at the corner for a while, and moved from a convex portion to a concave one on the surface with changing curvature.

Even in a simple system described above, a highly advanced control of the big-particle motion could be made. In biological systems, the geometric features of the membrane (surface) and proteins (big particles) are much more complex, and a highly sophisticated control would be made possible. It is interesting to ask the following questions: What kind of controls are realized in biological systems?; and for what purposes are those controls made? Further studies are necessary to answer these questions.

8. EFFECTS OF SALTS AND COSOLUTE MOLECULES

8.1. Crucial importance of salts

The only factor which can possibly predominate over the entropic interaction is the electrostatic interaction. Between groups with significantly large charges of the same sign in pure water, for example, a strong electrostatic repulsion suppresses the entropic interaction. When salts are added, however, the charges are screened by the counter ions. The entropic interaction can play important roles in biological systems because NaCl is present. By a model analysis (112) we have recently shown the following: Even between highly charged macroparticles the entropic interaction becomes essential when the NaCl concentration exceeds ~0.1M (the NaCl concentration in biological systems is ~0.15M).

We have performed a statistical-mechanical analysis (109) of the salt effects on the solubility and structural stability of proteins. A striking result is that like-charged groups are driven to become closer together by the salt addition: The interaction between groups with charges in the same sign can be *attractive* when the salt concentration is quite high. This is related to the issue considered in Section 6.4. We then discuss the relevance to the salt effects experimentally observed for two typical examples. The first example is the conformational transition and the solubility decrease caused by the salt addition for peptides and proteins with many positively charged groups in the side chains, and the second one is the salt-induced B-Z transition of DNA with many negatively charged phosphates. In the first example, the ability of salt to cause the conformational transition is strongly dependent on anion species and follows the order $I^->Br^->Cl^-$. In the second example, the ability of salt to cause the structural transition is strongly dependent on cation species and follows the order $Na^+>K^+>Rb^+>Cs^+$. The ability becomes higher as the anionic size increases in the first example, whereas in the second one it becomes higher as the cationic size decreases. We have succeeded in providing physical interpretations of these experimental observations (109).

8.2. Effects of adding medium-size particles

We have found by a statistical-mechanical analysis (113) that the entropic interaction between big particles immersed in small particles is greatly influenced by the addition of medium-size particles even in a very small amount. The medium-size particles correspond to cosolute molecules which are larger than water molecules but smaller than biopolymers. It is interesting that the strength and range of the interaction is quite variable depending on the size and concentration of the medium-size particles (113, 114). It is probable that this property is also being utilized in the control of the behavior of biopolymers in biological systems.

Let us introduce an experimental result related to the effect of the medium-size particles. The amyloid fibrils are first stabilized by adding a small amount of trifluoroethanol (TFE) to aqueous solution. However, a further addition destabilizes the fibrils and make them dissolve (115). A similar behavior has been observed for the stability of the native structure of a protein (116). These initially puzzling results have been elucidated by our analysis (114) concerning the effect of the concentration of medium-size particles on the entropic interaction between big particles immersed in small particles. In the analysis,

the small, medium-size, and big particles correspond to water molecules, TFE molecules, and proteins or portions of a protein molecule, respectively.

8.3. Surface-induced phase transition and long-range surface force

There exists another phenomenon arising from a complex correlation between water and hydrophobic molecules. There are lots of confined spaces (i.e., spaces confined by a surface or between two surfaces) in biological systems. The behavior of a fluid in a confined space is totally different from that of bulk fluid. Let us consider hydrophobic surfaces immersed in aqueous solution containing hydrophobic molecules at extremely low concentration. The hydrophobic molecules are highly enriched near the surfaces. We have shown by a statistical-mechanical analysis that even under the condition where the bulk is thermodynamically stable as a single phase, two types of surface-induced phase transitions (117-120) (thin-thick transition and bridging transition) can occur and give rise to a long-range, attractive surface force. In the bridging transition, for example, the space confined between hydrophobic surfaces is abruptly filled by hydrophobic molecules once the surface separation becomes as small as a threshold value. The attractive surface force then becomes quite strong, making the two surfaces stick together. In future studies, the roles of the surface-induced phase transitions in biological systems are to be investigated.

9. PERSPECTIVE

The variety of self-assembling and ordering processes occurring in biological systems accompany a large loss of the conformational and translational entropies of biomolecules. However, most of the loss is compensated by the entropic gain or the free-energy gain originating from the translational motion of the water molecules which are present in the system. The water entropy emphasized here is the translational entropy (or equivalently, the configurational entropy: a measure of the number of accessible configurations of the water). The entropy of the whole system including water molecules does not necessarily decrease: Even when it decreases, the energy gain required to overcome the entropic loss is much smaller in the presence of water. Many of the recently reported experimental data have shown that even in the isobaric process the enthalpy and entropy changes upon protein folding (61), amyloid-fibril formation (110), receptor-ligand binding (molecular recognition) (93, 94), and virus association (121), are both positive. This indicates that these processes are entropically driven: The primary driving force is the translational motion of water molecules.

In particular, Terazima and coworkers (61) have recently shown by novel experimental techniques that the folding of apoplastocyanin (apoPC) accompanies a very large enthalpic loss. It follows that an even larger entropic gain occurs in stabilizing the folded structure. We have theoretically calculated the water-entropy gain upon the folding of apoPC (122). It is demonstrated that the calculated value is in quantitatively good accord with the value estimated from the experimental data by accounting for the conformational-entropy loss. According to a prevailing view, the water adjacent to a hydrophobic group is unstable especially in terms of the rotational entropy and the folding is driven primarily by the release of such unfavorable water to the bulk through the burial of nonpolar side chains. We have shown, however, that the resultant entropic gain is too small to elucidate the experimental result. The great entropic gain observed is ascribed to the reduction of the restriction for the translational motion of water molecules in the whole system.

Thanks to the hydrogen bonding, water can exist in liquid (dense fluid) state at ambient temperature and pressure despite its exceptionally small molecular size. The entropic excluded volume effect, which stems from the translational motion of solvent molecules, is the largest for water among ordinary liquids in nature. This is an important answer to the question: Why is water indispensable to life? The roles of water can never be understood only by distinguishing the hydrophobic groups from the hydrophilic ones. The lattice model and the continuum model for water are not capable of accounting for the entropic effect. If the effect is considered more seriously, breakthrough will be attained for a number of problems related to biological systems.

The entropic effect arises not only from the water structure near a protein but also from the whole water in the system. In computer simulation for a protein immersed in water, for taking the entropic effect into account, the number of water molecules surrounding the protein is to be large enough. Moreover, they must be allowed to move for a sufficiently long time. These requirements could readily be met in the usual molecular dynamics (MD) simulations if the protein structure is fixed. In simulating the folding process, however, the time scale is to be sufficiently long so that the root mean square displacement of water molecules can be comparable with the protein size. The practical simulation time of 10^{-8}–10^{-6} sec could be too short. In a real system, it takes at least 10^{-3} sec for a small protein to fold. Another notable example is the simulation of pressure denaturation of a protein considered in Section 4.8. Paliwal *et al.* (81) have studied the pressure-induced denaturation by an MD simulation. They initiated the simulation by inserting water molecules into the protein interior and applying a high pressure afterward. This is because the water penetration cannot occur in the practical simulation time. This is why the statistical-mechanical methods such as the integral equation methods we have employed are quite important (much more powerful than the MD simulations in many studies).

When two Japanese one-yen coins whose surfaces are contaminated and become hydrophobic are floated on water, they contact each other due to the capillary force which is attractive and becomes stronger with decreasing surface separation. When one more one-yen coin is floated, the three coins contact one another so that the three centers form a regular triangle. It may look as if the one-yen coins *themselves* had the ability of making the s*elf-arrangement*, but this is not the case. The water plays the leading part. Even if one investigated the one-yen coins alone very carefully (e.g., if one analyzed the surface of the one-yen coin) to uncover the mechanism of the self-arrangement, nothing would become clear.

As described so far, statistical mechanics and thermodynamics with the emphasis on water can be very powerful tools in the investigation of biological systems and life. In future studies, we intend to extend the angle-dependent integral equation theory (24-32) to analyses on the hydration thermodynamics of a protein with the all-atom potentials. The resulting theory, which is the three-dimensional version, is not combined with the morphometric approach and the protein is explicitly treated. It is not suited for the prediction of the native structure of a protein because of a heavy computational burden, but it will be quite useful in detailed analyses on not only the changes of hydration thermodynamic quantities upon protein folding and unfolding but also their microscopic mechanisms. It is free from the drawback of the 3D-RISM theory (54, 55) that wrong predictions are obtained when the solute molecule is highly hydrophobic or the hydrophobic effect plays important roles (56).

Last, the simple free-energy function given by Equation (13), which is described in Section 4.6, has shed light on the development of a powerful method for predicting the native structure of a protein from its amino-acid sequence. No large computer memory is required in calculating the function and the computation time is only ~0.1 sec for one structure on the Itanium workstation. We are going to combine the function with the bioinformatics techniques to develop a practical tool for predicting the native structure. It is capable of handling large proteins and can also be extended to analyses of the protein-protein interaction and protein aggregation. The application to the drug design is also possible.

10. ACKNOWLEDGMENTS

The author wishes to thank his collaborators, Yuichi Harano (Sections 3.5, 4.1–4.8), Roland Roth (Sections 4.3, 4.4, and 4.6), Ryo Akiyama (Sections 3.5, 8.1, and 8.2), Nobuyuki Matubayasi (Section 3.8), Takashi Imai (Section 4.4), Mitsunori Ikeguchi (Section 4.6), Yuji Sugita (Section 4.6), and Takashi Yoshidome (Sections 4.8 and 4.9). They have made significant contributions in the subjects specified in the parentheses. Useful comments from Minoru Sakurai (on the molecular recognition), Mitsunori Ikeguchi (on the cold denaturation of proteins), and Koji Oda (on the prediction of the native structure of a protein) are greatly appreciated. The critical reading of the manuscript by Nobuyuki Matubayasi and Mitsunori Ikeguchi is gratefully acknowledged. This work was supported by Grants-in-Aid for Scientific Research on Priority Areas (No.15076203) from the Ministry of Education, Culture, Sports, Science and Technology of Japan and by the Next Generation Super Computing Project, Nanoscience Program, MEXT, Japan.

11. APPENDIX A: SOLVENT DENSITY PROFILE NEAR A SOLVOPHOBIC SOLUTE

If the solute is modeled as a hard sphere in the presence of no attractive interaction with solvent molecules, a depleted layer within which the average solvent density is lower than the bulk solvent density is formed near the solute. Even when the reduced density profile $g(r)$, the density profile divided by the bulk density, is larger than 1 in the immediate vicinity of the solute, the average density of the layer can be smaller than the bulk density. For small solutes, however, the incorporation of the solute-solvent van der Waals attractive interaction leads to the different result that the average density of the layer is higher than the bulk density. Therefore, the partial molar volume (PMV) of methane, for example, is considerably smaller than its excluded volume (EV).

The average solvent density of the solute-induced layer is largely dependent on the solute size (31). Hereafter, we discuss the case where the solvent is water. When a small hydrophobic solute intrudes into water, the water structure neighboring the solute can reorganize by forming the clathrate-like geometry without sacrificing the intermolecular hydrogen bonds. When a large hydrophobic solute intrudes into water, however, it is impossible to maintain the hydrogen bonds in a similar way and the loss of the bonds is unavoidable. To keep the loss of the hydrogen bonds as small as possible, the average water density of the solute-induced layer is made significantly low even in the presence of the solute-water van der Waals attractive interaction. As a result, the PMV of a large, nonpolar solute can be larger than its EV. We treat such large solutes in Section 3.5.

As for a protein, many of the nonpolar groups in the side chains are considerably larger than methane. Moreover, several groups are often close together, forming hydrophobic portions with rather extended surfaces. Therefore, nonpolar groups in a protein correspond *to the large solute mentioned above rather than to the small solute like methane*. The discussion in Section 4.7 is based on this probability.

12. APPENDIX B: CONTACT OF SOLUTES IMMERSED IN WATER IN ISOBARIC PROCESS BELOW 277 K

As the temperature T becomes higher, more hydrogen bonds are broken. This effect (Effect 1) makes the number density of water higher. At the same time, however, the effective volume occupied by a water molecule increases due to the more energetic thermal motion of water molecules. This effect (Effect 2) makes the number density lower. A peculiar behavior of water is that its number density takes the maximum value at 277 K and the isobaric thermal expansion coefficient α is negative below 277 K. Below 277 K, as T becomes higher Effect 1 dominates. In other words, the number of hydrogen bonds decreases when the number density becomes higher, and the former increases when the latter becomes lower. Above 277 K, however, Effect 2 dominates: The number of hydrogen bonds decreases when the number density becomes lower, and the former increases when the latter becomes higher.

Below 277 K, due to the peculiar behavior of water mentioned above, the statements in Cases (3) and (4) are to be modified:

3. Contact of solvophobic solutes in isobaric process: When Case (1) is regarded as the reference, a system-volume compression occurs and the number density becomes higher. Since the number of hydrogen bonds decreases, the energy gain becomes smaller. Due to the reduction of the constraint by the hydrogen bonds, the entropic gain becomes larger.

4. Contact of solvophilic solutes in isobaric process: When Case (2) is regarded as the reference, a system-volume expansion occurs and the number density becomes lower. Since the number of hydrogen bonds increases, the energy loss becomes smaller. Due to the enhancement of the constraint by the hydrogen bonds, the entropic gain becomes smaller.

In Case (3) the compression leads to the entropic gain and in Case (4) the expansion causes the entropic loss. This initially surprising behavior, which is deduced from Equations (5) and (6) with negative α, can thus be understood.

13. APPENDIX C. THE FIRST COEFFICIENT IN THE MORPHOMETRIC FORM FOR VARIOUS COMPONENTS OF HYDRATION ENTROPY

Let "S_{AO}+S_{PC}" be the solute-water pair correlation component of the hydration entropy in the isochoric process. S_{AO} is the term that is dependent only on the excluded volume and S_{PC} is the sum of the other terms (24, 52). S_{AO} is calculated using the Asakura-Oosawa theory (1, 2). The sum of the solute-water-water triplet and higher-order correlation components (24, 52) is denoted by S_{HC}. The contributions from the translational and rotational restrictions to S_{PC} and S_{HC} are represented by the subscripts "t" and "r", respectively. We then discuss the first coefficient C_1 in the case where the morphometric form of Equation (9) is applied to S_{AO}, S_{PCt}, S_{PCr}, S_{HCt}, or S_{HCr} (these are scaled by k_B). The important results are the following: C_1=0 for S_{PCt}, S_{PCr}, and S_{HCr}; $|C_1|$ for S_{HCt} >> $|C_1|$ for S_{AO}. S_{PCt}, S_{PCr}, and S_{HCr} are dependent only on the area and curvature of the water-accessible surface. Therefore, they are determined by the water structure near the solute. However, S_{HCt} has a term which depends on the excluded volume (EV). This implies that S_{HCt} is influenced by all the water molecules that are present in the system. (In S_{HCt}, the first EV-dependent term and the other three terms in the morphometric form are interdependent (52).)

In the isobaric process, the contributions from the rotational restriction remain unchanged (24) but those from the translational restriction are different. For example, there is no term which is dependent on the EV in the solute-water pair correlation component of the hydration entropy, because the system volume expands by the partial molar volume of the solute (24, 32, 52, 123). However, there is still an EV-dependent term in the sum of the solute-water-water triplet and higher-order correlation components. Therefore, by contrast to the conventional view, the hydration entropy cannot be scaled by the water-accessible surface area even in the isobaric process.

The gain or loss of the translational entropy of water upon the structural change of a protein must be considered in terms of all the water molecules that are present in the system. This is in contrast with the gain or loss of the rotational entropy which originates only from the water molecules near the protein surface.

14. REFERENCES

1. S. Asakura and F. Oosawa: On interaction between two bodies immersed in a solution of macromolecules. *J Chem Phys* 22, 1255-1256 (1954)

2. S. Asakura and F. Oosawa: Interaction between particles suspended in solutions of macromolecules. *J Polymer Sci* 33, 183-192 (1958)

3. T. Biben, P. Bladon, and D. Frenkel: Depletion effects in binary hard-sphere fluids. *J Phys: Condens Matter* 8, 10799-10821 (1996)

4. R. Dickman, P. Attard, and V. Simonian: Entropic forces in binary hard sphere mixtures: Theory and simulation. *J Chem Phys* 107, 205-213 (1997)

5. R. Roth, R. Evans, and S. Dietrich: Depletion potential in hard-sphere mixtures: Theory and applications. *Phys Rev E* 62, 5360-5377 (2000)

6. M. Kinoshita: Spatial distribution of a depletion potential between a big solute of arbitrary geometry and a big sphere immersed in small spheres. *J Chem Phys* 116, 3493-3501 (2002)

7. M. Kinoshita: Roles of entropic excluded-volume effects in colloidal and biological systems: Analyses using the three-dimensional integral equation theory. *Chem Eng Sci* 61, 2150-2160 (2006)

8. R. Roth and M. Kinoshita: Depletion potential between large spheres immersed in a multi-component mixture of small spheres. *J Chem Phys* 125, 084910(1-6) (2006)

9. J.-P. Hansen and I. R. McDonald – Theory of simple liquids. London: *Academic Press*, 3rd ed. (2005)

10. M. Kinoshita: Interaction between surfaces with solvophobicity or solvophilicity immersed in solvent: Effects due to addition of solvophobic or solvophilic solute. *J Chem Phys* 118, 8969-8981 (2003)

11. A. P. Minton: Influence of excluded volume upon macromolecular structure and associations in 'crowding' media. *Curr Opin Biotechnol* 8, 65-69 (1997)

12. R. J. Ellis and A. P. Minton: Cell biology: Join the crowd. *Nature* 425, 27-28 (2003)

13. M. Kinoshita, S. Iba, and M. Harada: Interaction between macroparticles in aqueous electrolytes. *J Chem Phys* 105, 2487-2499 (1996)

14. A. D. Dinsmore, A. G. Yodh, and D. J. Pine: Phase diagrams of nearly hard-sphere binary colloids. *Phys Rev E* 52, 4045-4057 (1995)

15. P. D. Kaplan, J. L. Rouke, A. G. Yodh, and D. J. Pine: Entropically driven surface phase separation in binary colloidal mixtures. *Phys Rev Lett* 72, 582-585 (1994)

16. A. D. Dinsmore, A. G. Yodh, and D. J. Pine: Entropic control of particle motion using passive surface microstructure. *Nature* 383, 239-242 (1996)

17. J. C. Crocker, J. A. Matteo, A. D. Dinsmore, and A. G. Yodh: Entropic attraction and repulsion in binary colloids probed with a line optical tweezer. *Phys Rev Lett* 82, 4352-4355 (1999)

18. M. Kinoshita, Y. Harano, and R. Akiyama: Changes in thermodynamic quantities upon contact of two solutes in solvent under isochoric and isobaric conditions, *J Chem Phys* 125, 244504(1-7) (2006)

19. L. Liu, C. Yang, and Q.-X. Guo: A study on the enthalpy-entropy compensation in protein unfolding. *Biophys Chem* 84, 239-251 (2000)

20. R. Lumry and S. Rajender: Enthalpy-entropy compensation phenomena in water solutions of proteins and small molecules – a ubiquitous property of water. *Biopolymers* 9, 1125-1128 (1970)

21. B. Lee: Enthalpy-entropy compensation in the thermodynamics of hydrophobicity. *Biophys Chem* 51, 271-278 (1994)

22. K. Sharp: Entropy-enthalpy compensation: Fact of artifact? *Protein Sci* 10, 661-667 (2001)

23. M. Kinoshita: Interaction between big bodies with high asphericity immersed in small spheres. *Chem Phys Lett* 387, 47-53 (2004)

24. M. Kinoshita: Molecular origin of the hydrophobic effect: Analysis using the angle-dependent integral equation theory. *J Chem Phys* 128, 024507(1-14) (2008)

25. P. G. Kusalik and G. N. Patey: On the molecular theory of aqueous electrolyte solutions. I. The solution of the RHNC approximation for models at finite concentration. *J Chem Phys* 88, 7715-7738 (1988)

26. P. G. Kusalik and G. N. Patey: The solution of the reference hypernetted-chain approximation for water-like models. *Mol Phys* 65, 1105-1119 (1988)

27. M. Kinoshita and M. Harada: Numerical solution of the RHNC theory for water-like fluids near a macroparticle and a planar wall. *Mol Phys* 81, 1473-1488 (1994)

28. M. Kinoshita and D. R. Berard: Analysis of the bulk and surface-induced structure of electrolyte solutions using integral equation theories. *J Comput Phys* 124, 230-241 (1996)

29. N. M. Cann and G. N. Patey: An investigation of the influence of solute size and insertion conditions on solvation thermodynamics. *J Chem Phys* 106, 8165-8195 (1997)

30. M. Kinoshita: Water structure and phase transition near a surface. *J Sol Chem* 33, 661-687 (2004)

31. M. Kinoshita: Density and orientational structure of water around a hydrophobic solute: Effects due to the solute size. *J Mol Liq* 119, 47-54 (2005)

32. M. Kinoshita, N. Matubayasi, Y. Harano, and M. Nakahara: Pair correlation entropy of hydrophobic hydration: Decomposition into translational and orientational contributions and analysis of solute-size effects. *J Chem Phys* 124, 024512(1-7) (2006)

33. G. Alagona and A. Tani: Structure of a dilute aqueous solution of argon. A Monte Carlo simulation. *J Chem Phys* 72, 580-588 (1980)

34. J. L. Finney and A. K. Soper: Solvent structure and perturbations in solutions of chemical and biological importance. *Chem Soc Rev* 23, 1-10 (1994)

35. R. A. Pierotti: Scaled particle theory of aqueous and non-aqueous solutions. *Chem Rev* 76, 717-726 (1976)

36. K. Soda: Solvent exclusion effect predicted by the scaled particle theory as an important factor of the hydrophobic effect. *J Phys Soc Jpn* 62, 1782-1793 (1993)

37. F. Hirata and P. J. Rossky: An extended RISM equation for molecular polar fluids. *Chem Phys Lett* 83, 329-334 (1981)

38. J. S. Perkyns and B. M. Pettitt: A site-site theory for finite concentration saline solutions. *J Chem Phys* 97, 7656-7666 (1992)

39. M. Kinoshita and F. Hirata: Application of the reference interaction site model theory to analysis on surface-induced structure of water. *J Chem Phys* 104, 8807-8815 (1996)

40. C. N. Pace: Polar group burial contribute more to protein stability than nonpolar group burial. *Biochemistry* 40, 310-313 (2001)

41. K. Takano, Y. Yamagata, S. Fujii, and K. Yutani: Contribution of the hydrophobic effect to the stability of human lysozyme: Calorimetric studies and X-ray structural analyses of the nine valine to alanine mutants. *Biochemistry* 36, 688-689 (1997)

42. M. Ikeguchi and J. Doi: Direct numerical solution of the Ornstein-Zernike integral equation and spatial distribution of water around hydrophobic molecules. *J*

Chem Phys 103, 5011-5017 (1995)

43. Y. Harano and M. Kinoshita: Large gain in translational entropy of water is a major driving force in protein folding. *Chem Phys Lett* 399, 342-348 (2004)

44. Y. Harano and M. Kinoshita: Translational-entropy gain of solvent upon protein folding. *Biophys J* 89, 2701-2710 (2005)

45. R. L. Baldwin: In search of the energetic role of peptide hydrogen bonds. *J. Biol. Chem.* 278, 17581 (2003)

46. Y. Snir and R. D. Kamien: Entropically driven helix formation. *Science* 307, 1067 (2005)

47. A. J. Doig and M. J. E. Sternberg: Side-chain conformational entropy in protein folding. *Protein Sci* 4, 2247-2251 (1995)

48. Y. Okamoto: Protein folding problem as studied by new simulation algorithms. *Recent Research Developments in Pure & Applied Chemistry* 2, 1- 22 Transworld Research Network, India (1998)

49. P. M. Konig, R. Roth, and K. R. Mecke: Morphological thermodynamics of fluids: Shape dependence of free energies. *Phys Rev Lett* 93, 160601(1-4) (2004)

50. R. Roth, Y. Harano, and M. Kinoshita: Morphometric approach to the solvation free energy of complex molecules. *Phys Rev Lett* 97, 078101(1-4) (2006)

51. H. J. C. Berendsen, J. R. Grigera, and T. P. Straatsma: The missing term in effective pair potentials. *J Phys Chem* 91, 6269-6271 (1987)

52. Y. Harano, T. Yoshidome, and M. Kinoshita: Molecular mechanism of pressure denaturation of proteins. *J Chem Phys* 129, 145103(1-9) (2008)

53. Y. Harano, R. Roth, and M. Kinoshita: On the energetics of protein folding in aqueous solution. *Chem Phys Lett* 432, 275-280 (2006)

54. T. Imai, Y. Harano, M. Kinoshita, A. Kovalenko, and F. Hirata: A theoretical analysis on changes in thermodynamic quantities upon protein folding: Essential roles of hydration. *J Chem Phys* 126, 225102(1-9) (2007)

55. T. Imai, Y. Harano, M. Kinoshita, A. Kovalenko, and F. Hirata: A theoretical analysis on hydration thermodynamics of proteins. *J Chem Phys* 125, 024911(1-7) (2006)

56. M. Kinoshita and Y. Harano: Characterization of models and theories of solvation using the morphometric approach. To be published in *J Chem Phys*

57. G. I. Makhatadze and P. L. Privalov: On the entropy of protein folding. *Protein Sci* 5, 507-510 (1996)

58. P. L. Privalov and N. N. Khechinashvili: Thermodynamic approach to problem of stabilization of globular protein structure: Calorimetric study. *J Mol Biol* 86, 665-684 (1974)

59. G. I. Makhatadze and P. L. Privalov: Contribution of hydration to protein-folding thermodynamics. 1. The enthalpy of hydration. *J Mol Biol* 232, 639-659 (1993)

60. P. L. Privalov and G. I. Makhatadze: Contribution of hydration to protein-folding thermodynamics. 2. The entropy and Gibbs energy of hydration. *J Mol Biol* 232, 660-679 (1993)

61. N. Baden, S. Hirota, T. Takabe, N. Funasaki, and M. Terazima: Thermodynamical properties of reaction intermediates during apoplastocyanin folding in time-domain. *J Chem Phys* 127, 175103(1-12) (2007)

62. T. Yoda, Y. Sugita, Y. Okamoto: Comparisons of force fields for proteins by generalized-ensemble simulations. *Chem Phys Lett* 386, 460-467 (2004)

63. Y. Harano, R. Roth, Y. Sugita, M. Ikeguchi, and M. Kinoshita: Physical basis for characterizing native structures of proteins. *Chem Phys Lett* 437, 112-116 (2007)

64. S. F. Sneddon, D. J. Tobias, and C. L. Brooks III: Thermodynamics of amide hydrogen bond formation in polar and apolar solvents. *J Mol Biol* 209, 817-820 (1989)

65. I. M. Klotz and S. B. Farnham: Stability of an amide-hydrogen bond in an apolar environment. *Biochemistry* 7, 3879-3882 (1968)

66. B. Park and M. Levitt: Energy functions that discriminates X-ray and near-native folds from well-constructed decoys. *J Mol Biol* 258, 367-392 (1996)

67. A. D. MacKerell Jr. *et al.*: All-atom empirical potential for molecular modeling and dynamics studies of proteins. *J Phys Chem B* 102, 3586-3616 (1998)

68. B. N. Dominy and C. L. Brooks III: Identifying native-like protein structures using physics-based potentials. *J Comput Chem* 23, 147-160 (2002)

69. B. R. Brooks, R. E. Bruccoleri, B. D. Olafson, D. J. States, S. Swaminathan, and M. Karplus: A program for macromolecular energy, minimization, and dynamics calculations. *J Comput Chem* 4, 187-217 (1983)

70. M. Feig, J. Karanicolas, and C. L. Brooks III: MMTSB Tool Set: Enhanced sampling and multiscale modeling methods for applications in structural biology. *J Mol Graphics Modell* 22, 377-395 (2004)

71. J. G. Kirkwood and F. P. Buff: The statistical mechanical theory of solutions. 1. *J Chem Phys* 19, 774-777 (1951)

72. Y. Harano and M. Kinoshita: On the physics of pressure denaturation of proteins. *J Phys: Condens Matter* 18, L107-L113 (2006)

73. Y. Harano and M. Kinoshita: Crucial importance of translational entropy of water in pressure denaturation of proteins. *J Chem Phys* 125, 024910(1-10) (2006)

74. K. Kuwamoto and M. Kinoshita: Interaction between solute molecules in medium density solvents. *Mol Phys* 98, 725-736 (2000)

75. M. L. Connolly: Analytical molecular surface calculation. *J Appl Crystallog* 16, 548-558 (1983)

76. G. Panick, G. J. A. Vidugiris, R. Malessa, G. Rapp, R. Winter, and C. A. Royer: Exploring the temperature-pressure phase diagram of staphylococcal nuclease *Biochemistry* 38, 4157-4164 (1999)

77. J. Woenckhaus, R. Kohling, P. Thiyagarajan, K. C. Litterell, S. Seifert, C. A. Royer, and R. Winter: Pressure-jump small-angle X-ray scattering detected kinetics of staphylococcal nuclease folding. *Biophys J* 80, 1518-1523 (2001)

78. C. A. Royer: Revisiting volume changes in pressure-induced protein unfolding. *Biochim Biophys Acta, Prot Struct Mol Enzymol* 1595, 201-209 (2002)

79. G. S. Chryssomallis, P. M. Torgerson, H. G. Drickamer, and G. Weber: Effect of hydrostatic-pressure on lysozyme and chymotrypsinogen detected by fluorescence polarization. *Biochemistry* 20, 3955-3959 (1981)

80. C. Clery, F. Renault, and P. Masson: Pressure-induced molten globule state of cholinesterase. *FEBS Lett* 370, 212-214 (1995)

81. A. Paliwal, D. Asthagiri, D. P. Bossev, and M. E. Paulaitis: Pressure denaturation of staphylococcal nuclease studied by neutron small-angle scattering and molecular simulation. *Biophys J* 87, 3479-3492 (2004)

82. G. Hummer, S. Garde, A. E. Garcia, M. E. Paulaitis, and L. R. Pratt: The pressure dependence of hydrophobic interactions is consistent with the observed pressure denaturation of proteins. *Proc Natl Acad Sci USA* 95, 1552-1555 (1998)

83. A. C. Oliveira, L. P. Gaspar, A. T. Da Poian, and J. L. Silva: ARC repressor will not denature under pressure in the absence of water. *J Mol Biol* 240, 184-187 (1994)

84. D. Paschek and A. E. Garcia: Reversible temperature and pressure denaturation of a protein fragment: A replica exchange molecular dynamics simulation study. *Phys Rev Lett* 93, 38105(1-4) (2004)

85. W. W. Wood and J. D. Jacobson: Preliminary results from a recalculation of the Monte Carlo equation of state of hard spheres. *J Chem Phys* 27, 1207-1208 (1957)

86. B. J. Alder and T. E. Wainwright: Phase transition for a hard sphere system. *J Chem Phys* 27, 1208-1209 (1957)

87. P. N. Pusey and W. van Megen: Phase behaviour of concentrated suspensions of nearly hard colloidal spheres. *Nature* 320, 340-342 (1986)

88. P. L. Privalov, Y. V. Griko, S. Y. Venyaminov: Cold denaturation of myoglobin. *J Mol Biol* 190, 487-498 (1986)

89. A. Pastore, S. R. Martin, A. Politou, K. C. Kondapalli, T. Stemmler, and P. A. Temussi: Unbiased cold denaturation: Low- and high-temperature unfolding of yeast frataxin under physiological conditions. *J Am Chem Soc* 129, 5374-5375 (2007)

90. J. Fitter: A measure of conformational entropy change during thermal protein unfolding using neutron spectroscopy. *Biophys J* 84, 3924-3930 (2003)

91. T. Yoshidome and M. Kinoshita: Molecular mechanism of cold denaturation of proteins. To be published in *Biophys J*

92. M. Kinoshita and T. Oguni: Depletion effects on the lock and key steric interactions between macromolecules. *Chem Phys Lett* 351, 79-84 (2002)

93. H. Ohtaka, A. Schon, and E. Freire: Multidrug resistance to HIV-1 protease inhibition requires cooperative coupling between distal mutations. *Biochemistry* 42, 13659-13666 (2003)

94. W. E. Stites: Protein-protein interactions: Interface structure, binding thermodynamics, and mutational analysis. *Chem Rev* 97, 1233-1250 (1997)

95. M. Lopez de la Paz, K. Goldie, J. Zurdo, E. Lacroix, C. M. Dobson, A. Hoenger, and L. Serrano: De novo designed peptide-based amyloid fibrils. *Proc Natl Acad Sci USA* 99, 16052-16057 (2002)

96. R. Tycko: Insights into the amyloid folding problem from solid-state NMR. *Biochemistry* 42, 3151-3159 (2003)

97. C. Goldsbury, J. Kistler, U. Aebi, T. Arvinte, and G. J. S. Cooper: Watching amyloid fibrils grow by time-lapse atomic force microscopy. *J Mol Biol* 285, 33-39 (1999)

98. M. Sunde, L. C. Serpell, M. Bartlam, P. E. Fraser, M. B. Pepys, and C. C. F. Blake: Common core structure of amyloid fibrils by synchrotron X-ray diffraction. *J Mol Biol* 273, 729-739 (1997)

99. K. Hasegawa, I. Yamaguchi, S. Omata, F. Gejyo, and H. Naiki: Interaction between Aβ(1-42) and Aβ(1-40) in Alzheimer's β-amyloid fibril formation *in vitro*. *Biochemistry* 38, 15514-15521 (1999)

100. L. C. Serpell, M. Sunde, M. D. Benson, G. A. Tennent, M. B. Pepys, and P. E. Fraser: The protofilament

substructure of amyloid fibrils. *J Mol Biol* 300, 1033-1039 (2000)

101. L. Nielsen, R. Khurana, A. Coats, S. Frokjaer, J. Brange, S. Vyas, V. N. Uversky, and A. L. Fink: Effect of environmental factors on the kinetics of insulin fibril formation: Elucidation of the molecular mechanism. *Biochemistry* 40, 6036-6046 (2001)

102. J. Goers, S. E. Permyakov, E. A. Permyakov, V. N. Uversky, and A. L. Fink: Conformational prerequisites for α-lactalbumin fibrillation. *Biochemistry* 41, 12546-12551 (2002)

103. D.-P. Hong, M. Gozu, K. Hasegawa, H. Naiki, and Y. Goto: Conformation of β_2-microglobulin amyloid fibrils analyzed by reduction of the disulfide bond. *J Biol Chem* 277, 21554-21560 (2002)

104. M. Hoshino, H. Katou, Y. Hagihara, K. Hasegawa, H. Naiki, and Y. Goto: Mapping the core of the β_2-microglobuli amyloid fibril by H/D exchange. *Nature Struc Biol* 9, 332-336 (2002)

105. T. Ban, D. Hamada, K. Hasegawa, H. Naiki, and Y. Goto: Direct observation of amyloid fibril growth monitored by thioflavin T fluorescence. *J Biol Chem* 278, 16462-16465 (2003)

106. M. Kinoshita: Ordered aggregation of big bodies with high asphericity in small spheres: A possible mechanism of the amyloid fibril formation. *Chem Phys Lett* 387, 54-60 (2004)

107. M. Kinoshita: A physical picture of the amyloid fibril formation. Proceedings of the 10th APCChE (Asian Pacific Confederation of Chemical Engineering) Congress, Kitakyushu International Conference Center, Japan, October 17-21, 2004, 1P-07-054

108. B. Raman, E. Chatani, M. Kihara, T. Ban, M. Sakai, K. Hasegawa, H. Naiki, Ch. M. Rao, and Y. Goto: Critical balance of electrostatic and hydrophobic interactions is required for β_2–microglobulin amyloid fibril growth and stability. *Biochemistry* 44, 1288-1299 (2005)

109. M. Kinoshita and Y. Harano: Potential of mean force between solute atoms in salt solution: Effects due to salt species and relevance to conformational transition of biomolecules. *Bull Chem Soc Jpn* 78, 1431-1441 (2005)

110. J. Kardos, K. Yamamoto, K. Hasegawa, H. Naiki, and Y. Goto: Direct measurement of the thermodynamic parameters of amyloid formation by isothermal titration calorimetry. *J Biol Chem* 279, 55308-55314 (2004)

111. K. Akasaka, A. R. Abdul Latif, A. Nakamura, K. Matsuo, H. Tachibana, and K. Gekko: Amyloid protofibril is highly voluminous and compressible. *Biochemistry* 46, 10444-10450 (2007)

112. R. Akiyama, N. Fujino, K. Kaneda, and M. Kinoshita: Interaction between like-charged colloidal particles in aqueous solution: Attractive component arising from solvent granularity", *Condens Matter Phys* 10, 587-596 (2007)

113. M. Kinoshita: Interaction between large spheres immersed in small spheres: Remarkable effects due to a trace amount of medium-sized spheres. *Chem Phys Lett* 353, 259-269 (2002)

114. R. Akiyama, Y. Karino, Y. Hagiwara, and M. Kinoshita: Remarkable solvent effects on depletion interaction in crowding media: Analyses using the integral equation theories. *J Phys Soc Jpn* 75, 064804(1-7) (2006)

115. N. Hirota-Nakaoka, K. Hasegawa, H. Naiki, and Y. Goto: Dissolution of beta(2)-microglobulin amyloid fibrils by dimethylsulfoxide. *J Biochem* 134, 159-164 (2003)

116. N. Youhnovski, I. Matecko, M. Samalikova, and R. Grandri: Characterization of cytochrome c unfolding by nano-electrospray ionization time-of-flight and Fourier transform ion cyclotron resonance mass spectrometry. *J Mass Spectrom* 11, 519-524 (2005)

117. M. Kinoshita: Long-range attractive interaction between macroparticles in a binary fluid mixture. *Mol Phys* 94, 485-494 (1998)

118. M. Kinoshita: Binary fluid mixture confined between macroparticles: Surface-induced phase transition and long-range surface forces. *Chem Phys Lett* 325, 281-287 (2000)

119. M. Kinoshita: Effects of a trace amount of hydrophobic molecules on phase transition for water confined between hydrophobic surfaces: Theoretical results for simple models. *Chem Phys Lett* 326, 551-557 (2000)

120. M. Kinoshita: Surface-induced phase transition and long-range surface force: Roles in colloidal and biological systems. *Recent Research Developments in Molecular Physics* 1, 21-41, Transworld Research Network, India (2003)

121. C. F. S. Bonafe, C. M. R. Vital, R. C. B. Telles, M. C. Goncalves, M. S. A. Matsuura, F. B. T. Pessine, D. R. C. Freitas, and J. Vega: Tabacco mosaic virus disassembly by high hydrostatic pressure in combination with urea and low temperature. *Biochemistry* 37, 11097-11105 (1998)

122. T. Yoshidome, M. Kinoshita, S. Hirota, N. Baden, and M. Terazima: Thermodynamics of apoplastocyanin folding: Comparison between experimental and theoretical results. *J Chem Phys* 128, 225104(1-9) (2008)

123. H. S. Ashbaugh and M. E. Paulaitis: Entropy of hydrophobic hydration: extension to hydrophobic chains. *J Phys Chem* 100, 1900-1913 (1996)

Abbreviations: AO: Asakura-Oosawa, ASA: solvent-accessible surface area, CE: conformational entropy, EV: excluded volume, PMF: potential of mean force, PMV: partial molar volume, RISM: reference interaction site model, 3D-RISM: three-dimensional RISM, SFE: solvation free energy, TE: translational entropy

Key words: Water, Life, Entropy, Translational Motion, Self-Assembly, Ordering Process, Protein Folding, Molecular Recognition, Biomolecules, Excluded Volume, Accessible Surface Area, Integral Equation Theory, Liquid State Theory, Molecular Liquids, Morphometric Thermodynamics, Entropic Force, Hydrophobicity, Solvation Thermodynamics, Solvation Free Energy, Partial Molar Volume, Enthalpy-Entropy Compensation, Hydration, Dehydration, Pressure Denaturation, Cold Denaturation, Aggregation, Amyloid Fibril, Alpha-Helix, Beta-Sheet, Side Chains, Native Structure, Conformational Entropy, Hydrogen Bonds, Multipolar Model, Surface Force, Colloidal Suspension, Depletion Potential, Potential Of Mean Force, Lock-Key Interaction, Receptor, Ligand, Dna, B-Z Transition, Actin, Lipid, Biological Membrane, Selectivity, Regularity, Symmetry, Phase Transition, Salt Effect, Isochoric Process, Isobaric Process, Review

Send correspondence to: Masahiro Kinoshita, Institute of Advanced Energy, Kyoto University, Uji, Kyoto 611-0011, Japan. Tel.: 81-774-38-3503, Fax: 81-774-38-3508, E-mail: kinoshit@iae.kyoto-u.ac.jp

http://www.bioscience.org/current/vol14.htm